



## In situ FTIR and XANES studies of thiophene hydrodesulfurization on Ni<sub>2</sub>P/MCM-41

S. Ted Oyama<sup>a,b</sup>, Travis Gott<sup>a</sup>, Kiyotaka Asakura<sup>c,\*</sup>, Satoru Takakusagi<sup>c</sup>, Kotaro Miyazaki<sup>b</sup>, Yuichiro Koike<sup>d</sup>, Kyoko K. Bando<sup>e,\*</sup>

<sup>a</sup> Environmental Catalysis and Materials Laboratory, Department of Chemical Engineering, Virginia Polytechnic Institute and State University, Blacksburg, VA 24061-0211, USA

<sup>b</sup> Department of Chemical Systems Engineering, Tokyo University, Hongo 7-3-1, Tokyo, Japan

<sup>c</sup> Catalysis Research Center, Hokkaido University, Kita 21-10, Kita-ku, Sapporo 001-0021, Japan

<sup>d</sup> Photon Factory, Institute of Structure Material Science, High Energy Accelerator Research Organization, (KEK-PF), Oho 1-1, Tsukuba 305-0811, Japan

<sup>e</sup> National Institute of Advanced Industrial Science and Technology, 1-1-1, Higashi, Tsukuba 305-8565, Japan

### ARTICLE INFO

#### Article history:

Received 13 July 2009

Revised 20 September 2009

Accepted 23 September 2009

Available online 10 November 2009

#### Keywords:

FTIR

XANES

Hydrodesulfurization

Thiophene

Nickel phosphide

Ni<sub>2</sub>P

ACT

In situ

### ABSTRACT

The hydrodesulfurization (HDS) of thiophene was studied over Ni<sub>2</sub>P/MCM-41 by in situ Fourier transform infrared (FTIR) spectroscopy and X-ray absorption near-edge structure (XANES) measurements at atmospheric pressure and 393–723 K (120–450 °C). FTIR showed the presence of adsorbed molecular thiophene principally on the MCM-41 support. In the presence of hydrogen new bands in the aliphatic C–H stretching region (2953, 2918, and 2876 cm<sup>-1</sup>) and the CH<sub>2</sub> scissoring region (1464 cm<sup>-1</sup>) appeared and grew with temperature up to 553 K (280 °C). These were assigned to a tetrahydrothiophene surface intermediate, whose presence is consistent with the high hydrogenation activity of nickel phosphide. XANES measurements between 353 and 573 K (180–300 °C) also showed growth of a signal (8330.9 eV) attributed to Ni–S interactions of either the adsorbed tetrahydrothiophene or a surface phosphosulfide. Transient XANES measurements showed that the sulfur species responded dynamically at the same rate as the steady-state rate, indicating that it was associated with an intermediate in the reaction.

© 2009 Elsevier Inc. All rights reserved.

### 1. Introduction

Recently, hydrodesulfurization (HDS), an industrial process used to remove sulfur from petroleum feedstocks, has come to prominence because of world-wide legislation limiting the amount of sulfur in transportation fuels and the decline in quality of crude feedstocks [1,2]. Fourier transform infrared spectroscopy (FTIR) [3–8] and extended X-ray absorption fine-structure (EXAFS) [9–14] have been applied to the investigation of hydrotreating catalysts, but little work has been previously done on the analysis of the reaction mechanisms.

The catalyst used in this study is a novel material, Ni<sub>2</sub>P/MCM-41. Transition metal phosphides are a new class of catalyst showing extremely high activity for HDS and hydrodenitrogenation reactions with better performance than commercial sulfide catalysts [15,16]. The subject has been recently reviewed [1]. Among the phosphides, nickel phosphide has been found to be particularly active [17–21]. Previous in situ EXAFS studies of Ni<sub>2</sub>P/SiO<sub>2</sub> showed the formation of stable clusters with surface Ni–S bonds during HDS [22–24]. In the case of Ni<sub>2</sub>P/MCM-41, EXAFS has shown the

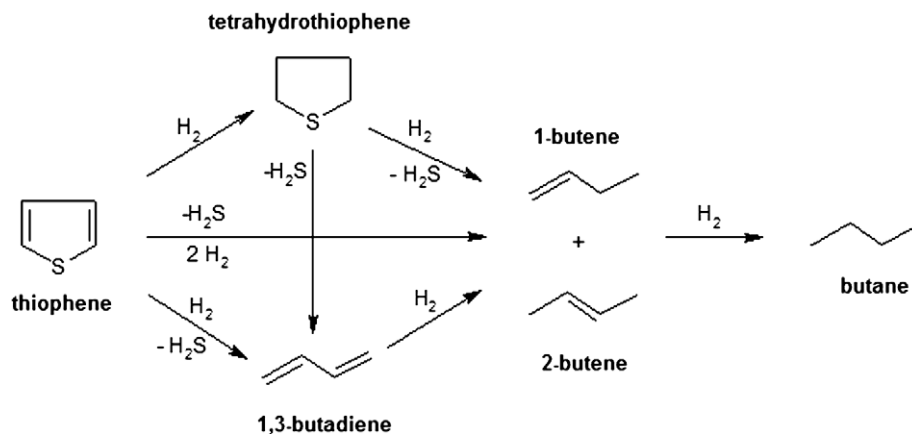
formation of small Ni<sub>2</sub>P clusters dispersed on the support, which expose primarily square-pyramidal sites [25]. These sites are particularly active for hydrogenation.

Thiophene is often used as a model compound for the study of the mechanism and kinetics of HDS as it is the simplest of the aromatic sulfur compounds in crude oil. Examination of the bonding and reaction of thiophene on catalysts' surfaces affords the opportunity to study the most important steps of HDS, namely hydrogenation, cleavage of C–S bonds, and removal of sulfur as H<sub>2</sub>S. However, the reaction mechanism for the HDS of thiophene remains a matter of great debate. From an extensive review of the literature, a global reaction network was proposed by Topsøe and co-workers as shown in Scheme 1 [26]. Similar to the HDS of larger S-containing compounds such as 4,6-dimethyldibenzothiophene, both a direct C–S bond cleavage and a hydrogenation pathway with hydrogenation of one or both C=C bonds prior to C–S bond scission have been proposed [26–28].

As can be seen, several pathways for the removal of sulfur from thiophene likely coexist. In addition, both surface reaction and hydrogenative removal of sulfur have been proposed to be rate-determining [29]. The governing reaction pathway and rate-controlling step depend on the catalyst, temperature, and H<sub>2</sub> pressure [26,60]. The mode of thiophene adsorption has also been covered extensively in the literature and several modes have been

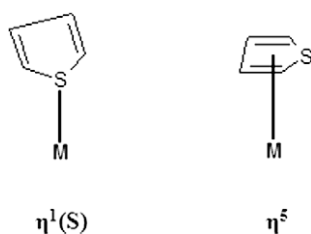
\* Corresponding authors.

E-mail addresses: [askr@cat.hokudai.ac.jp](mailto:askr@cat.hokudai.ac.jp) (K. Asakura), [kk.bando@aist.go.jp](mailto:kk.bando@aist.go.jp) (K.K. Bando).



proposed from studies of thiophene bonding in organometallic complexes [30,31]. Scheme 2 illustrates the generally accepted adsorption modes of thiophene to metal sites on the surface of hydrotreating catalysts –  $\sigma$ -bonded thiophene through the sulfur atom (upright,  $\eta^1(\text{S})$ ) and  $\pi$ -bonded thiophene (parallel,  $\eta^5$ ) [32]. However, the mode of adsorption that activates thiophene toward further reaction is unclear [33]. Several studies have provided evidence of both  $\sigma$ - [34] and  $\pi$ -bonds [35] thiophene as possible precursors. In addition, the mode of adsorption has been suggested to be coverage dependent. In several single crystal experiments the preferred mode was thought to be flat orientation with  $\pi$ -bonding at low coverages and upright via a  $\sigma$ -bond between the sulfur atom and a metal center at higher coverages [36,37]. Other single crystal work has shown that the mode of adsorption is coverage independent [38].

Directly monitoring the surface coverage of an adsorbed surface species during adsorption and reaction is a powerful tool for elucidating kinetic and mechanistic information [39,40]. Such studies involve measuring the rates of adsorption and reaction under transient conditions and comparing the transient rates with the overall reaction rate measured under steady-state conditions, a method that has been denoted as the Analysis of Coverage Transients (ACTs) [41]. Agreement between the separately measured rates constitutes proof that the observed intermediate is a true reaction intermediate and is kinetically significant in the global mechanism. The present study employs in situ FTIR of adsorption and reaction of thiophene over  $\text{Ni}_2\text{P}/\text{MCM-41}$  to probe the bonding mode of thiophene and products formed during HDS at atmospheric pressure over a range of temperatures. Moreover, in situ, time-resolved analysis of XANES features (Ni K-edge) during adsorption and reaction of thiophene is used to investigate the interaction of thiophene with the catalyst surface. Changes in the intensity of a pre-edge feature below the adsorption edge that correlates with the local coordination chemistry around the absorbing atom are followed [42], and indicate the involvement of a tetrahydrothiophene intermediate or a surface phosphosulfide.



## 2. Experimental section

### 2.1. Synthesis and characterization

The supports used in this study were siliceous MCM-41 and  $\text{SiO}_2$  (Cabosil, EH-5 Grade). The mesoporous MCM-41 silica support was synthesized following a literature procedure [43]. The chemicals used in the synthesis were colloidal silica (Fluka, HS-40), cetyltrimethylammonium bromide (CTMABr, Aldrich, 99%), and tetramethylammonium hydroxide (TMAOH, Aldrich, 25 wt.% aqueous solution). The CTMABr and TMAOH were added to deionized water with stirring at 300 K until the solution became transparent, then the colloidal silica was added to the solution with stirring for 1 h and the resulting reaction gel was aged for 24 h at 323 K. The molar composition was 1.0  $\text{SiO}_2$ : 0.27 CTMABr: 0.19 TMAOH: 40  $\text{H}_2\text{O}$ . After aging, the mixture was reacted for 48 h at 393 K in a Teflon-lined stainless steel autoclave. The product was filtered, washed with distilled water, dried in air at 393 K, and finally calcined at 623 K for 8 h. The catalyst precursors were nickel nitrate hexahydrate,  $\text{Ni}(\text{NO}_3)_2 \cdot 6\text{H}_2\text{O}$  (Alfa Aesar, 99%), and ammonium hydrogen phosphate,  $(\text{NH}_4)_2\text{HPO}_4$  (Aldrich, 99%). Thiophene (Aldrich, 99%) was used in the study of hydrodesulfurization over the supported  $\text{Ni}_2\text{P}$  catalysts. All chemicals were used as received. The gases employed were He (Airgas, UPC grade),  $\text{H}_2$  (Airgas, UPC grade),  $\text{N}_2$  (Airgas, UPC grade), and CO (Airgas, Linde Research Grade, 99.97%). The gases were passed through two-stage gas purifiers (Alltech, model 4658) to remove moisture and oxygen. Additionally, 0.5%  $\text{O}_2/\text{He}$  (Airgas, UHP), which was used for passivation of reduced samples, was passed through a purifier to remove moisture.

The supported  $\text{Ni}_2\text{P}$  catalyst was prepared with excess phosphorus ( $\text{Ni}/\text{P} = 1/2$ ) and a metal loading of 1.15 mmol  $\text{Ni g}_{\text{support}}^{-1}$  (12.2 wt.%  $\text{Ni}_2\text{P}/\text{support}$ ). The synthesis of the supported catalyst involved two steps. Briefly, in the first step, a supported nickel phosphate was prepared by incipient wetness impregnation of nickel and phosphorus precursors, followed by drying and calcination in static air. In the second step, the phosphate was reduced to phosphide in flowing  $\text{H}_2$  by temperature-programmed reduction (TPR). The synthesis of MCM-41-supported  $\text{Ni}_2\text{P}$  is presented below as an example.

Prior to use, the MCM-41 was dried at 393 K for 3 h and calcined at 813 K for 7 h. The incipient wetness point of the MCM-41 was found to be  $2.0 \text{ cm}^3 \text{ g}^{-1}$ . In the first step, 2.13 g (16.1 mmol) of  $(\text{NH}_4)_2\text{HPO}_4$  was dissolved in 5  $\text{cm}^3$  of distilled water to form a transparent colorless solution. Subsequently, 2.34 g (8.05 mmol) of  $\text{Ni}(\text{NO}_3)_2 \cdot 6\text{H}_2\text{O}$  was added to yield a lightly colored mixture with some precipitate. Several drops of concentrated  $\text{HNO}_3$  were added

to dissolve the precipitate and the solution was further diluted to a total volume of 14 cm<sup>3</sup>, resulting in a transparent green solution. The precursor solution was then impregnated on 7 g of MCM-41. After the impregnation, the powder was dried at 393 K for 6 h and calcined at 673 K for 4 h. The calcined material was ground with a mortar and pestle, pelletized with a press (Carver, Model C), crushed, and sieved to a particle diameter of 650–1180 μm (16/20 mesh). The supported nickel phosphate was reduced by TPR using a H<sub>2</sub> flow rate of 1000 cm<sup>3</sup> (NTP) min<sup>-1</sup> per g of sample. A portion of the gas effluent was sampled through a leak valve into a mass spectrometer (Ametek/Dycor Model MA100) and the masses 2 (H<sub>2</sub>), 4 (He), 18 (H<sub>2</sub>O), 28 (N<sub>2</sub>), 31 (P), and 34 (PH<sub>3</sub>) were monitored. After the temperature program, the sample was cooled to room temperature in flowing He and passivated in a flow of 0.5% O<sub>2</sub>/He for 4 h to prevent rapid oxidation of the freshly reduced phosphide.

The samples were characterized by BET surface area measurements (Micromeritics ASAP 2010), pulse CO chemisorption, powder X-ray diffractometry (XRD, Scintag XDS-2000 operated at 45 kV, and 40 mA with Cu K<sub>α</sub> monochromatized radiation). Irreversible CO uptake measurements at room temperature were used to titrate the surface metal atoms and provide an estimate of the active sites on the catalysts. Before the measurements, 0.3 g of passivated sample was placed in a U-shaped quartz reactor and rereduced in flowing H<sub>2</sub> (300 cm<sup>3</sup> (NTP) min<sup>-1</sup>) at 803 K for 2 h.

## 2.2. In situ FTIR measurements

Fourier transform infrared (FTIR) spectra were collected (Digilab Excalibur Series FTS 3000) with a combined reactor-spectrometer system (Fig. 1) using a low-volume in situ cell with water-cooled KBr windows. For all experiments, 32.5 mg of finely ground Ni<sub>2</sub>P/MCM-41 or pure MCM-41 was pressed into self-supporting wafers with a diameter of 13 mm (24.5 mg cm<sup>-2</sup>). The wafers were mounted vertically in a quartz sample holder to keep the incident IR beam normal to the samples. Rods of CaF<sub>2</sub> (13 mm

diameter) were placed on both sides of the samples to minimize interference by gas-phase thiophene and reduce the dead volume (20 cm<sup>3</sup>) of the in situ reactor. For the experiments, absorbance spectra were collected in the range 4000–1000 cm<sup>-1</sup> at a resolution of 4 cm<sup>-1</sup> with 64 scans per spectrum. Before dosing thiophene, the supported Ni<sub>2</sub>P or blank support sample was pretreated in H<sub>2</sub> for 2 h at 803 K (530 °C) at a flow rate of 130 cm<sup>3</sup> (NTP) min<sup>-1</sup>. After pretreatment, the samples were cooled in flowing He or H<sub>2</sub> (200 cm<sup>3</sup> (NTP) min<sup>-1</sup>) and background spectra were collected in the absence of thiophene at 723, 673, 593, 553, 513, and 393 K (450, 400, 320, 280, 240, and 120 °C). The samples were dosed at atmospheric pressure and 393 K (120 °C) with 1.0 mol% thiophene in He or H<sub>2</sub> carrier at a total flow rate of 200 cm<sup>3</sup> (NTP) min<sup>-1</sup> until saturation was achieved. Thiophene was delivered to the sample by passing carrier gas through a thiophene-filled bubbler immersed in a temperature-controlled water bath. The thiophene vapor pressure (3.69 kPa at 278 K) was obtained using the Antoine equation:

$$\log P^{\text{sat}} = A - \frac{B}{T + C} \quad (1)$$

where  $P^{\text{sat}}$  is the vapor pressure in mmHg,  $T$  is the bubbler temperature in °C, and the coefficients are 7.06944, 1296.79, and 225.437 for A, B, and C, respectively [44]. The vapor-phase concentration was adjusted to 1.0 mol% by blending the main carrier flow containing thiophene with a dilution gas stream to a total flow rate of 200 cm<sup>3</sup> (NTP) min<sup>-1</sup>. Spectra are shown with subtraction of the background contribution to highlight the thiophene adsorbate bands. Temperature was changed at a heating rate of 5 K min<sup>-1</sup> (0.083 K s<sup>-1</sup>). The reactor temperature was held constant at each temperature for 180 s to collect the corresponding spectrum under thiophene/carrier flow.

## 2.3. In situ XAS measurements

The in situ X-ray absorption spectroscopy (XAS) measurements were carried out at BL9C in the Photon Factory, Institute for Material Structure Science, High Energy Accelerator Organization

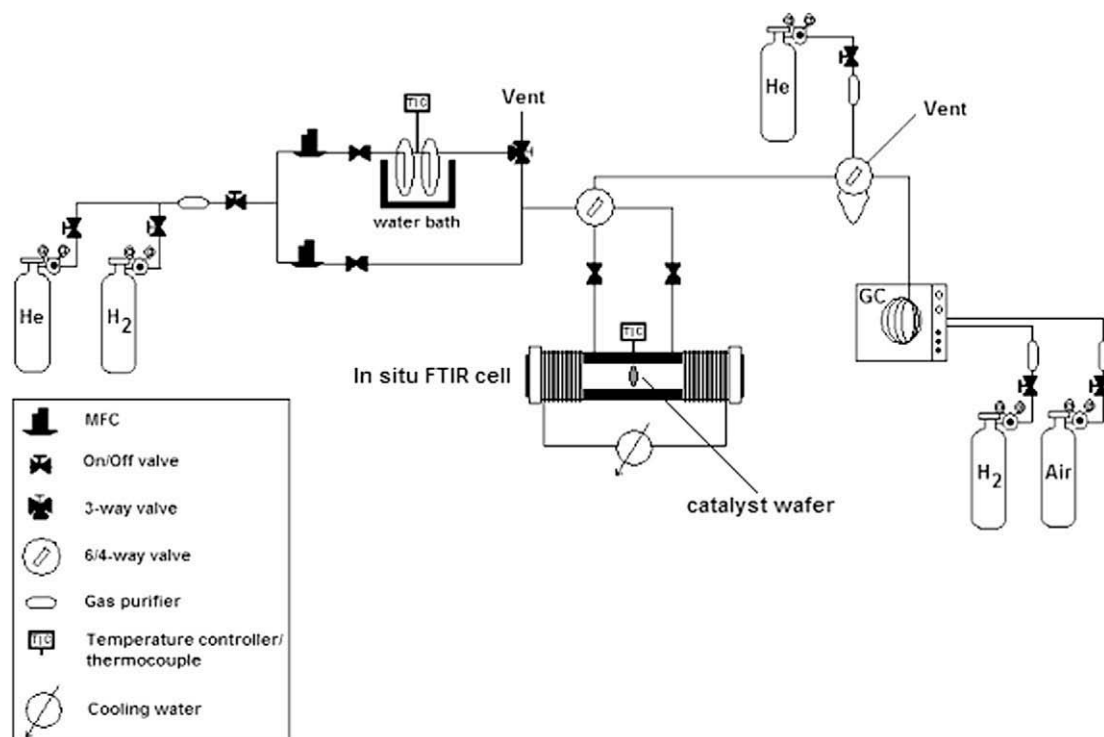


Fig. 1. In situ FTIR reactor system.

(KEK-IMSS-PF) with a ring energy of 2.5 GeV and a current of 450 mA. The X-rays passed through a Si(1 1 1) double crystal monochromator and were focused onto the sample by a bent-cylindrical mirror. The extended X-ray absorption fine-structure (EXAFS) and X-ray absorption near-edge structure (XANES) data were collected in transmission mode using  $I_0$  and  $I$  ionization chambers filled with 100%  $N_2$  and 15% Ar in  $N_2$ , respectively. Reaction gases were supplied by a gas-handling system [45].

A quantity of 47 mg of  $Ni_2P/MCM-41$  was pressed into a wafer of 10 mm in diameter and placed in an in situ EXAFS cell equipped with polyimide windows [22,23]. The sample was reduced as for the synthesis of the catalysts by temperature-programmed reduction to 803 K (530 °C) at  $5 K min^{-1}$ , while following the reduction with XANES. Following reduction and EXAFS analysis of the sample, adsorption or reaction measurements were carried out with thiophene in He (0.13 mol%) or in  $H_2$  (0.13 mol%) at atmospheric pressure and 453, 513, and 573 K (180, 240, and 300 °C). The sample was re-reduced at 803 K (530 °C) prior to each change in temperature or gas composition.

#### 2.4. Activity tests for thiophene HDS

Catalytic activity measurements of the HDS of thiophene were carried out in the aforementioned FTIR reactor (Fig. 1). For the measurements of steady-state turnover rates of thiophene over  $Ni_2P/MCM-41$ , the system was operated at atmospheric pressure with a gas-phase feed containing 0.13 mol% thiophene in  $H_2$  carrier. For all experiments, 47 mg of finely ground  $Ni_2P/MCM-41$  was pressed into a self-supporting wafer with a diameter of 13 mm ( $35.4 mg cm^{-2}$ ). Prior to the kinetic measurements, the  $Ni_2P/MCM-41$  sample was pretreated at 803 K for 2 h under  $130 cm^3 (NTP) min^{-1}$  of flowing  $H_2$  at atmospheric pressure and then cooled to the reaction temperature. Gas-phase thiophene was introduced to the reactor by passing  $H_2$  through a thiophene-filled bubbler immersed in a low temperature water bath. The Antoine equation was again used to obtain the thiophene vapor pressure (3.69 kPa at 278 K) and the concentration was adjusted to 0.13 mol% by blending the main carrier flow containing thiophene with a dilution  $H_2$  stream at a flow rate of  $100 cm^3 (NTP) min^{-1}$ . The reaction was allowed to stabilize for 6 h before sampling to ensure steady-state conditions. The reactor exit was directly connected to a 6-way sampling valve for on-line GC analysis of gaseous reactants and products. Steady-state conversions and product compositions were determined by on-line analysis with a gas chromatograph (Hewlett-Packard, 5890A) equipped with a 0.32 mm i.d.  $\times$  50 m dimethylsiloxane capillary column (CPSil-5CB, Chrompack, Inc.) and a flame ionization detector. The reactants and products were identified by matching retention times to standards injected separately. The reaction was conducted at several temperatures (453, 513, and 573 K) and several measurements were made at each condition to check the attainment of steady-state. A fresh sample wafer was used for each temperature to exclude the effects of deactivation of the sample during the experiments. The results of several injections at each temperature were averaged and used to calculate the turnover frequency from the following equation:

$$TOF = \frac{\text{thiophene flow rate } (\mu\text{mol/s}) \cdot \text{steady-state conversion}}{\text{catalyst weight (g)} \cdot \text{chemisorption uptake } (\mu\text{mol/g})} \quad (2)$$

### 3. Results

The MCM-41-supported  $Ni_2P$  catalyst was prepared by the temperature-programmed reduction of supported nickel phosphate

precursors. Fig. 2 shows the water evolution during the temperature-programmed reduction of phosphate to phosphide for the supported samples with an onset at 750 K. Masses P (31) and  $PH_3$  (34) followed the same trend as the  $H_2O$  (18) signal and are not shown here. For the  $Ni_2P/MCM-41$  catalyst sample a distinct reduction peak at 868 K is observed while for a  $Ni_2P/SiO_2$  sample of identical loading supported on a lower surface area support ( $130 m^2 g^{-1}$ ) the reduction peak shifts to higher temperature for the sample with higher support surface area and better dispersion.

Fig. 3 shows the reduction of the sample followed by Ni K-edge XANES. The arrows indicate the shifts in absorbance intensity during the course of reduction. The major feature is the white line peak at 8345.6 eV, which decreases in intensity with reduction. Other peaks after the white line at 8372.8, 8393.0, and 8426.9 eV mark the onset of the EXAFS oscillations. The pre-edge feature at 8330.9 eV gives information about Ni coordination and symmetry.

Fig. 4 shows the reduction of the sample as monitored by the intensity of the absorbance at 8330.9 eV. The absorbance signal starts increasing significantly after 120 min of reduction, which corresponds to a temperature of 750 K.

Table 1 lists the BET specific surface area and CO chemisorption uptake of the MCM-41-supported  $Ni_2P$  sample. Fig. 5 shows the powder XRD pattern of a reference  $Ni_2P/SiO_2$  sample and the

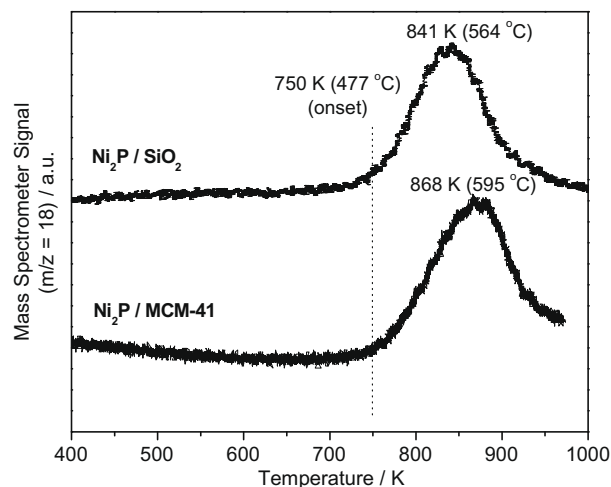


Fig. 2.  $M/Z = 18$  signal for TPR of the samples at  $\beta = 2 K min^{-1}$  ( $0.0333 K s^{-1}$ ).

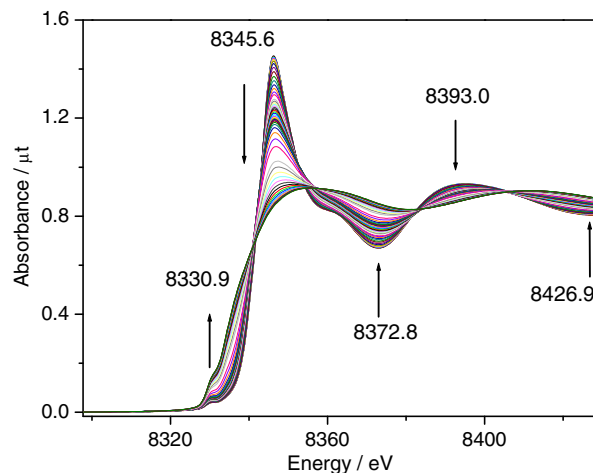


Fig. 3. Changes in the Ni K-edge XANES region in the reduction of  $Ni_2P/MCM-41$ .

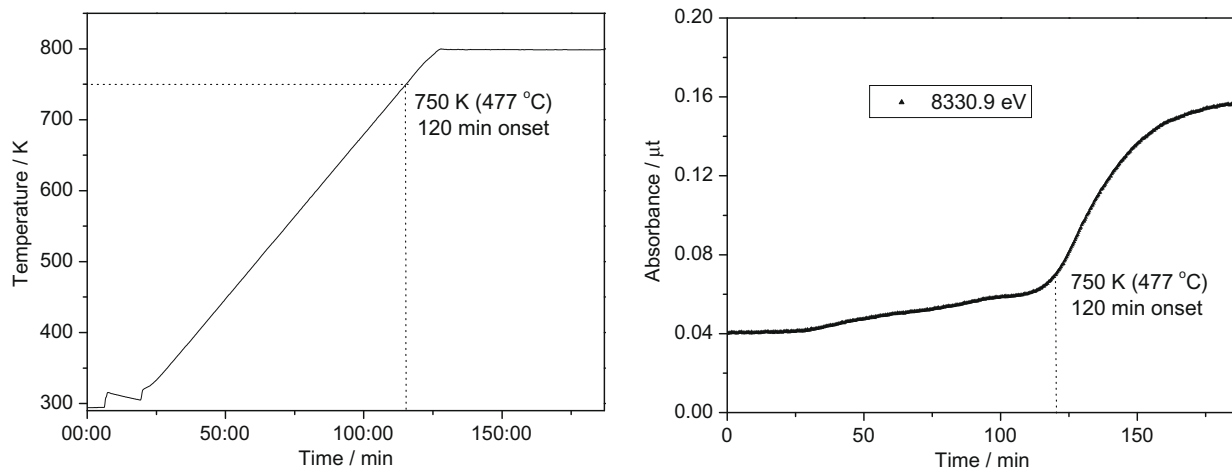


Fig. 4. Reduction of Ni<sub>2</sub>P/MCM-41 followed by XANES.

**Table 1**  
Physical properties of Ni<sub>2</sub>P/MCM-41.

Sample	BET surface area (m <sup>2</sup> g <sup>-1</sup> )	CO uptake (μmol g <sup>-1</sup> )	Metal dispersion (%)
Ni <sub>2</sub> P/MCM-41	487 (1076) <sup>a</sup>	188	16

<sup>a</sup> BET surface area of pure siliceous support.

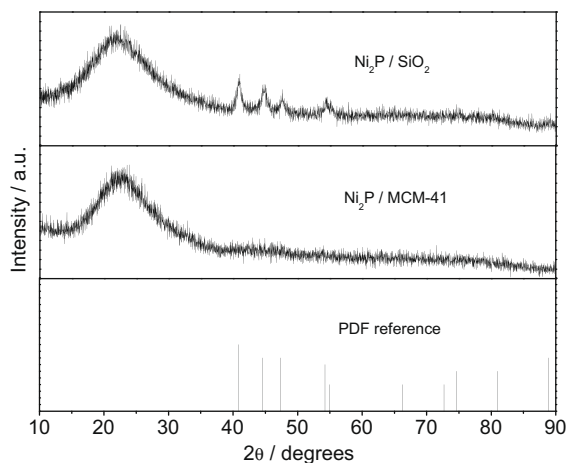


Fig. 5. XRD patterns of supported Ni<sub>2</sub>P catalysts.

Ni<sub>2</sub>P/MCM-41 catalyst after both reduction and passivation. Both patterns exhibit a broad peak at  $2\theta \sim 22^\circ$  due to the amorphous SiO<sub>2</sub> support and some amorphous domains in MCM-41 upon impregnation of the active phase. At higher angles the Ni<sub>2</sub>P/SiO<sub>2</sub> shows peaks at  $2\theta \sim 41^\circ$ ,  $45^\circ$ ,  $48^\circ$ , and  $55^\circ$  due to the Ni<sub>2</sub>P phase (bottom panel), but the Ni<sub>2</sub>P/MCM-41 sample exhibits no peaks, indicating a high dispersion of the Ni<sub>2</sub>P crystallites.

Fig. 6 shows the powder XRD patterns at low angles of the calcined MCM-41 support and the freshly prepared Ni<sub>2</sub>P/MCM-41 catalyst. The MCM-41 support exhibits typical features, an intense line at  $2\theta \sim 2.5^\circ$  and three weak diffraction lines at  $2\theta \sim 4.1^\circ$ ,  $4.6^\circ$ , and  $6.1^\circ$ . The Ni<sub>2</sub>P/MCM-41 sample shows a decrease in intensity and broadening of the (1 0 0) reflection and disappearance of the higher order reflections.

Fig. 7 shows the FTIR spectra of the pure MCM-41 support under 1 mol% thiophene/He flow. The left and right panels show the

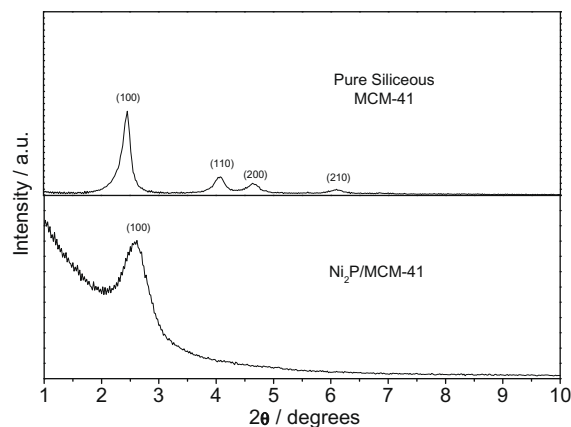


Fig. 6. Low-angle XRD patterns of MCM-41 and Ni<sub>2</sub>P/MCM-41.

$\nu_{C-H}$  region ( $3200\text{--}2800\text{ cm}^{-1}$ ) and low wavenumber region, respectively. The spectra under 1 mol% thiophene/H<sub>2</sub> flow are not shown as they exhibit identical absorbance features. In the  $\nu_{C-H}$  region several small bands were located at 3134, 3125, 3109, 3098, 3090, and 3082  $\text{cm}^{-1}$ . With increasing temperature, no changes in the intensities of the bands were observed. No discernible bands were detected in the  $3000\text{--}2800\text{ cm}^{-1}$  range of the spectrum. In the low wavenumber region the main spectral features were located at 1622, 1584, 1574, 1491, 1454, 1420, 1410, and 1400  $\text{cm}^{-1}$ . The intensities of the bands at 1622, 1491, and 1454  $\text{cm}^{-1}$  were observed to increase slightly from 393 to 553 K and decrease monotonically up to 723 K. The intensities of all other features were invariant with increasing adsorption temperature. After degassing in He flow for 300 s only bands at 1622, 1491, and 1454  $\text{cm}^{-1}$  remained at 393 K (spectra not shown).

Fig. 8 shows the FTIR spectra after background subtraction of thiophene adsorbed on Ni<sub>2</sub>P/MCM-41 in 1 mol% thiophene/He flow at high wavenumbers with the right panel highlighting the  $\nu_{C-H}$  region of the spectra. Two absorbance bands at 3742 and 3665  $\text{cm}^{-1}$  appear as negative features and correspond to surface hydroxyl groups of siliceous MCM-41 and P-OH. In the  $\nu_{C-H}$  region ( $3200\text{--}2800\text{ cm}^{-1}$ ) there are several small features on a rising background found at 3134, 3125, 3107, 3098, 3090, and 3082  $\text{cm}^{-1}$ . In addition, several broad, weak absorbance bands are clearly observed below 3000  $\text{cm}^{-1}$ . The features in the  $3200\text{--}3000\text{ cm}^{-1}$  are assigned to aromatic  $\nu_{C-H}$  absorbances while the weak features in the  $3000\text{--}2800\text{ cm}^{-1}$  region are attributed to aliphatic  $\nu_{C-H}$  modes. With

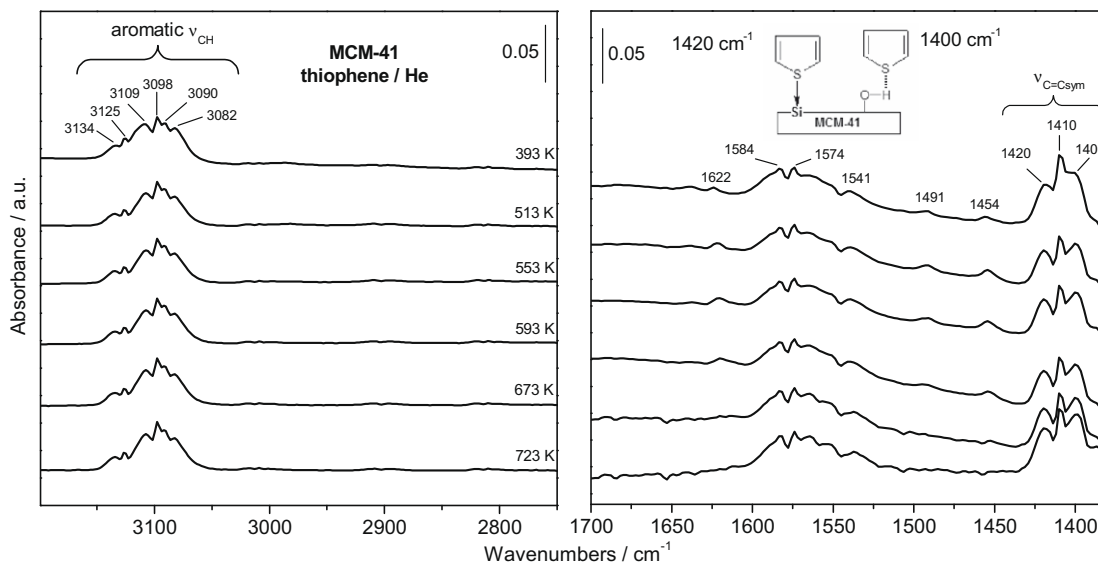


Fig. 7. FTIR spectra of thiophene adsorbed on MCM-41 in thiophene/He flow as a function of temperature.

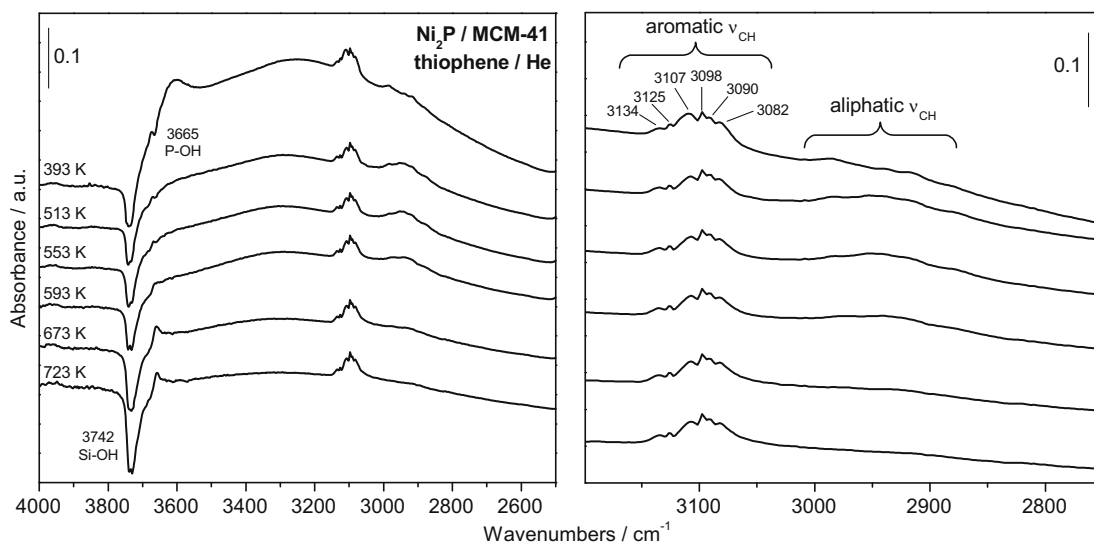


Fig. 8. FTIR spectra of thiophene adsorbed on Ni<sub>2</sub>P/MCM-41 in thiophene/He flow as a function of temperature (high wavenumber region).

increasing temperature, the hydroxyl band at 3742 cm<sup>-1</sup> increases in negative intensity while the negative band at 3665 cm<sup>-1</sup> decreases in intensity and actually becomes a positive feature above 593 K. The positive bands between 3134 and 3082 cm<sup>-1</sup> remain relatively unchanged up to 723 K. The intensities of the broad features below 3000 cm<sup>-1</sup> increase slightly from 393 to 553 K but diminish rapidly at higher temperatures.

Fig. 9 shows the FTIR spectra in the low wavenumber region corresponding to those of Fig. 8 of thiophene adsorbed on Ni<sub>2</sub>P/MCM-41 in 1 mol% thiophene/He flow. The right panel highlights the ν<sub>(C=C)sym</sub> region of the spectra. The main spectral features were located at 1611, 1584, 1574, 1541, 1491, and 1450 cm<sup>-1</sup>. In the 1450–1380 cm<sup>-1</sup> range, additional bands are located at 1420, 1410, and 1400 cm<sup>-1</sup>. Identification of absorbance features in the 1700–1450 cm<sup>-1</sup> region was difficult due to poor signal-to-noise ratio. However, features at 1653, 1636, 1560, and 1506 cm<sup>-1</sup> were clearly observed at 393 K. Upon highlighting the ν<sub>(C=C)sym</sub> region a weak band at 1437 cm<sup>-1</sup> was also observed at 393 K.

Fig. 10 shows the FTIR spectra at high wavenumbers of thiophene adsorbed on Ni<sub>2</sub>P/MCM-41 in 1 mol% thiophene/H<sub>2</sub> flow with the right panel highlighting the ν<sub>C-H</sub> region of the spectra. Two negative bands at 3740 and 3667 cm<sup>-1</sup> due to hydroxyl groups were again observed. Similar to the spectra obtained in He carrier the feature at 3740 cm<sup>-1</sup> was retained up to 723 K while the intensity of the feature at 3667 cm<sup>-1</sup> decreased with increasing temperature. The weak features due to aromatic ν<sub>CH</sub> modes at 3136, 3125, 3107, 3098, 3090, and 3080 cm<sup>-1</sup> were again observed. The other major spectral features included three new bands with high intensity centered at 2953, 2918, and 2876 cm<sup>-1</sup> assigned to aliphatic ν<sub>CH</sub> modes of absorption, which increased in intensity as the temperature was raised from 393 to 553 K.

Fig. 11 shows the FTIR spectra of thiophene adsorbed on Ni<sub>2</sub>P/MCM-41 in 1 mol% thiophene/H<sub>2</sub> flow at low wavenumbers, with the right panel highlighting the ν<sub>(C=C)sym</sub> region of the spectra. The main spectral features were located at 1638, 1601, 1491, 1449, 1420, 1410, and 1400 cm<sup>-1</sup>. The bands are very similar to

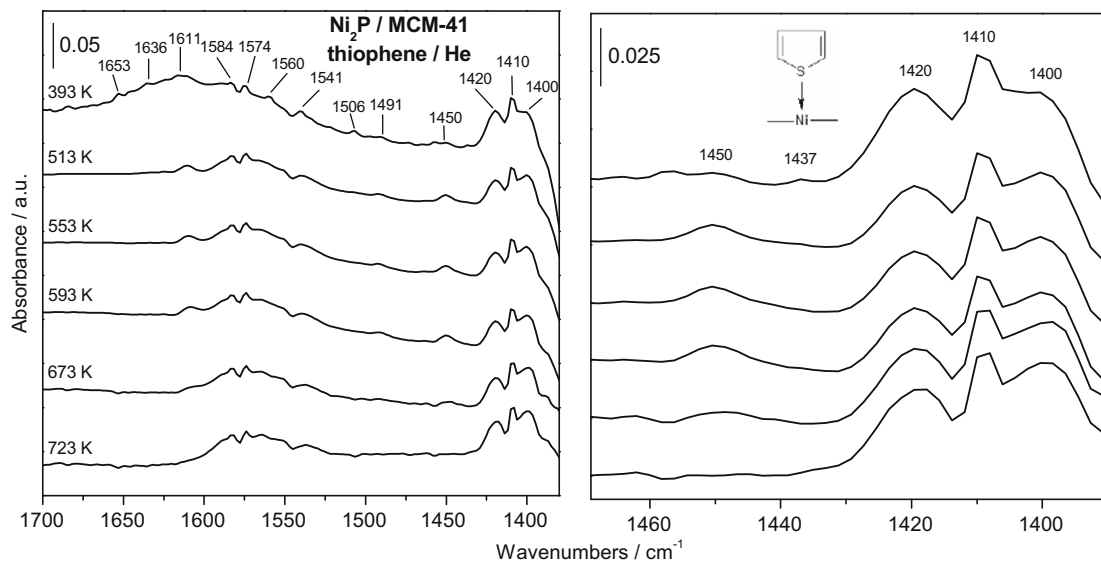


Fig. 9. FTIR spectra of thiophene adsorbed on Ni<sub>2</sub>P/MCM-41 in thiophene/He flow as a function of temperature (low wavenumber region).

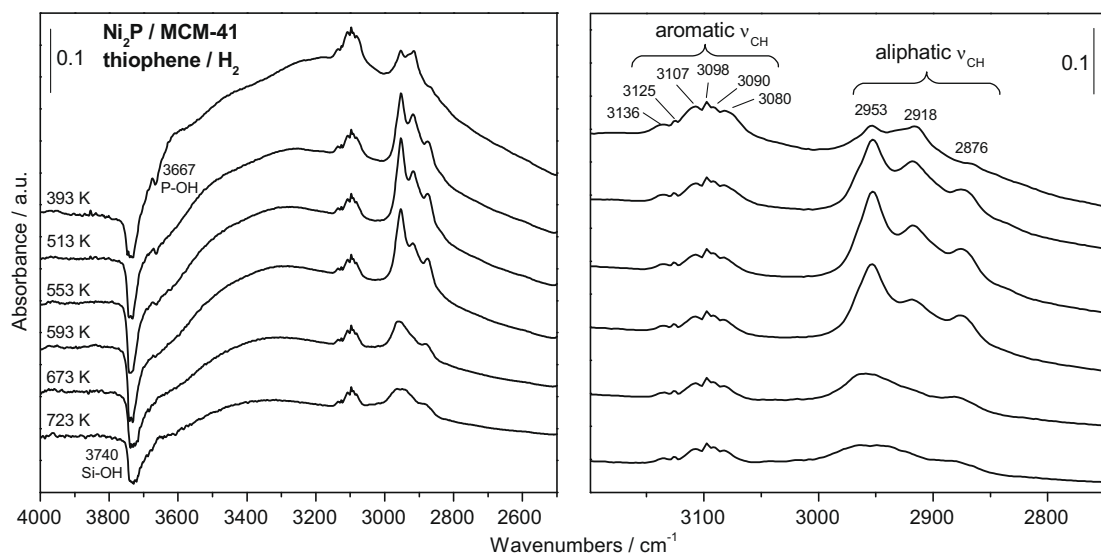


Fig. 10. FTIR spectra of thiophene adsorbed on Ni<sub>2</sub>P/MCM-41 in thiophene/H<sub>2</sub> flow as a function of temperature (high wavenumber region).

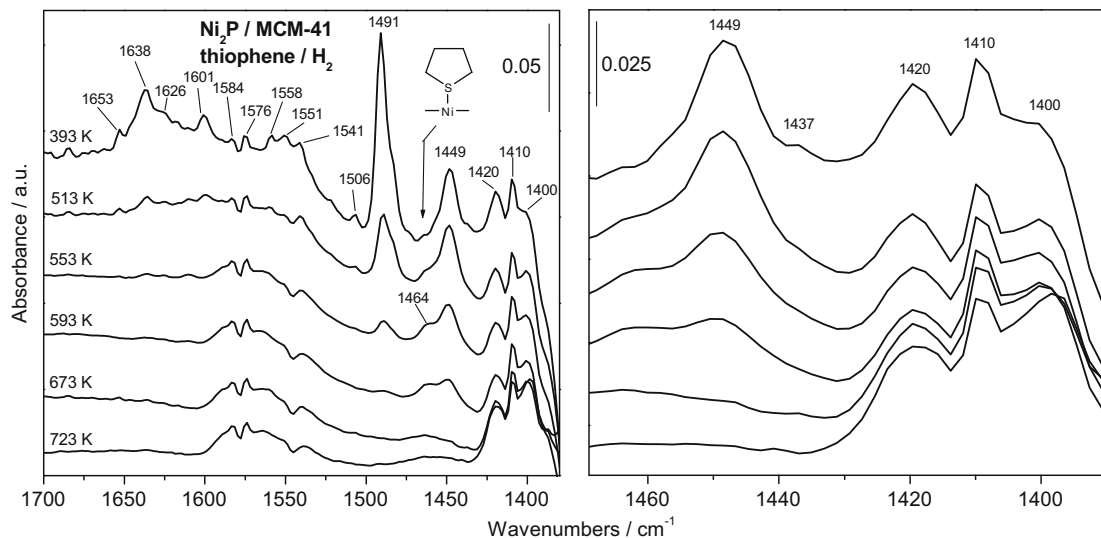


Fig. 11. FTIR spectra of thiophene adsorbed on Ni<sub>2</sub>P/MCM-41 in thiophene/H<sub>2</sub> flow as a function of temperature (low wavenumber region).

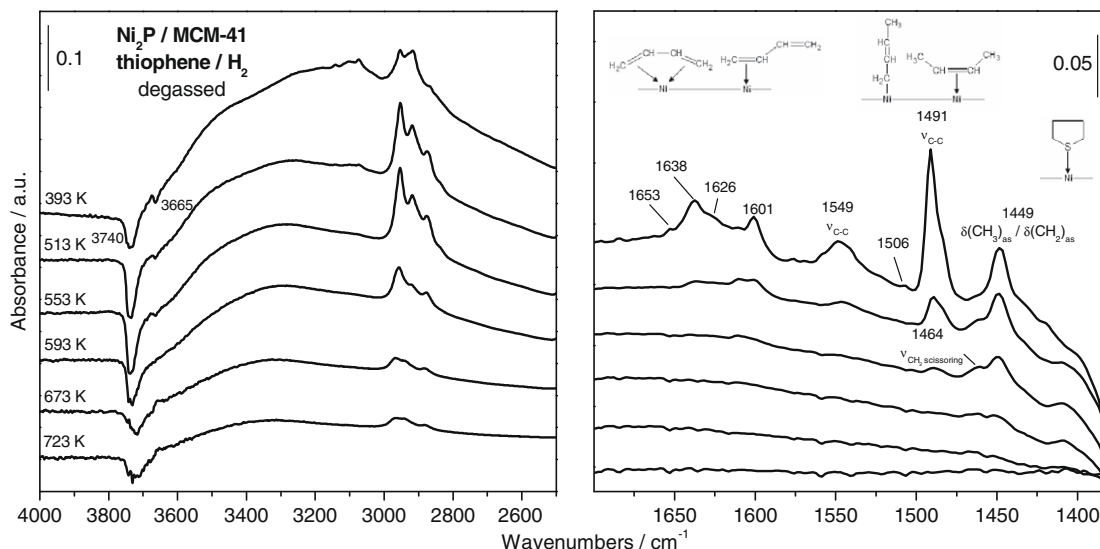


Fig. 12. FTIR spectra of thiophene adsorbed on Ni<sub>2</sub>P/MCM-41 after 300 s degassing in H<sub>2</sub> flow as a function of temperature.

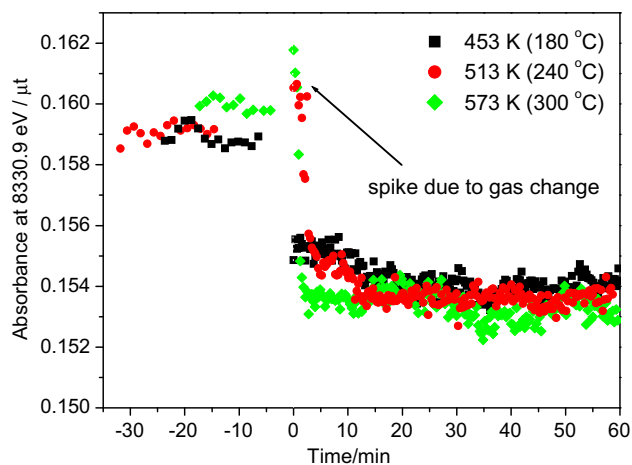


Fig. 13. XANES measurements of the Ni<sub>2</sub>P/MCM-41 sample exposed to thiophene/H<sub>2</sub> (0.13 mol%).

those obtained under He flow but the features at 1491 and 1449 cm<sup>-1</sup> are much more intense. Additional smaller bands centered at 1653, 1638, 1626, 1584, 1576, 1558, 1551, 1541, 1506,

and 1464 cm<sup>-1</sup> were observed in the 1700–1460 cm<sup>-1</sup> range. In the  $\nu_{(C=C)_{sym}}$  region of the spectra a small band at 1437 cm<sup>-1</sup> is again observed. An increase in the temperature led to a decrease in the intensity of bands located at 1653, 1638, 1626, 1601, 1506, 1491, and 1449 cm<sup>-1</sup> while all other bands were retained up to 723 K. The band at 1464 cm<sup>-1</sup>, which appears as a shoulder on the feature at 1449 cm<sup>-1</sup>, was observed to grow in intensity with heating from 393 to 553 K. At higher temperature the intensity of the feature diminished rapidly.

Fig. 12 shows the changes in the FTIR spectra at high (left panel) and low (right panel) wavenumbers for thiophene adsorbed on Ni<sub>2</sub>P/MCM-41 following 300 s of degassing in H<sub>2</sub>. Once again, bands located between 3136 and 3080 were diminished in intensity and undetectable above 393 K. The three strong bands at 2953, 2918, and 2876 cm<sup>-1</sup> were retained following degassing although with slightly reduced intensity. In the low wavenumber region bands at 1653, 1638, 1626, 1601, 1506, 1491, 1464, and 1449 cm<sup>-1</sup> were retained after degassing in H<sub>2</sub> at 393 K. The intensities of the two strong bands at 1491 and 1449 cm<sup>-1</sup> were maintained, but diminished rapidly with heating. The feature at 1464 cm<sup>-1</sup> was again observed to increase with heating up to 553 K and diminish at higher temperatures. In addition, a new band at 1549 cm<sup>-1</sup> was observed.

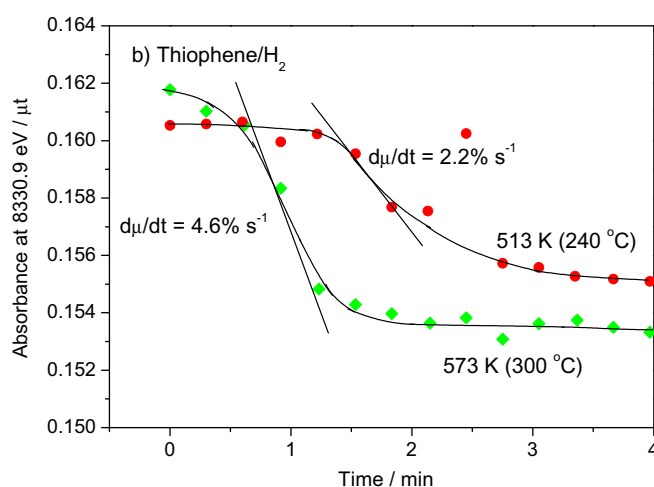
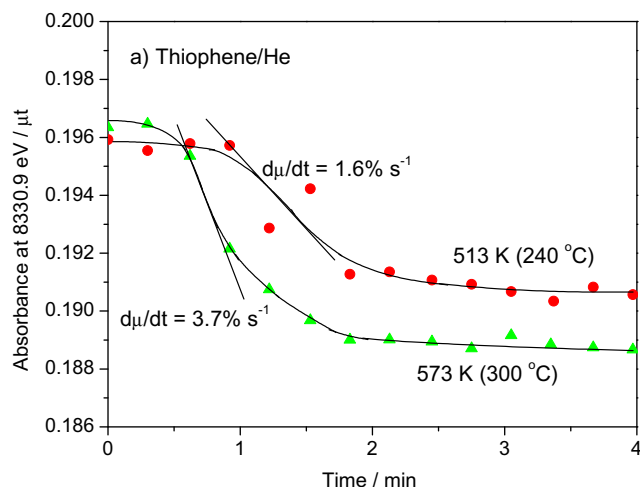


Fig. 14. Decline in absorbance at 8330.9 eV for thiophene adsorption. (a) Thiophene/He = 0.13 mol% and (b) thiophene/H<sub>2</sub> = 0.13 mol%.

Fig. 13 shows XANES measurements of the Ni<sub>2</sub>P/MCM-41 sample exposed to thiophene/H<sub>2</sub> mixtures (time zero) at different temperatures. The absorbance at 8330.9 eV shows a rapid decrease in intensity to steady values that are indicative of the interaction of thiophene with the catalyst. The spike at time zero is an artifact due to the switch in gas streams.

Fig. 14 compares the initial decline in absorbance at 8330.9 eV due to thiophene adsorption in H<sub>2</sub> and He carriers. The absorbance values are slightly different in the two carrier gases because of the absorbance characteristics of both gases. The decline in absorbance

is higher at higher temperature. Also indicated are the slopes at the inflection points of the curves, which will be discussed later.

Fig. 15 shows XANES traces obtained in isothermal and temperature-programmed experiments with adsorbed thiophene on samples that have been reduced at 530 °C before each change in condition. The left part of each figure shows the isothermal region in which thiophene is desorbed in either He or H<sub>2</sub> at 453, 513, or 573 K (180, 240, or 300 °C). The increase in absorbance indicates a decline in Ni–S coordination consistent with desorption. In all cases the signal reaches a plateau, indicating the termination of the process. The right side of each figure shows the signal in the temperature-programmed part of the experiment, where there is a further increase in signal. Analysis of the results, explained later, indicates removal of further sulfur.

## 4. Discussion

### 4.1. Catalyst properties

The MCM-41-supported Ni<sub>2</sub>P catalyst was prepared by the temperature-programmed reduction of supported nickel phosphate precursors. The precursor was prepared with four times the stoichiometric amount of phosphorous (Ni/P = 1/2) necessary to form Ni<sub>2</sub>P. Previous work had shown that excess phosphorus was required to synthesize an active catalyst since some phosphorus is lost during the reduction of phosphate to phosphide [4,17,18]. Samples prepared with phosphorus quantities closer to stoichiometric proportions were found to form inactive phosphorus-deficient phases such as Ni<sub>12</sub>P<sub>5</sub> [46]. When P levels were increased above stoichiometric quantities an active Ni<sub>2</sub>P was formed, whose activity in dibenzothiophene HDS did not change substantially with P content. This indicated that the extra P was located on the support, and did not affect the composition of the Ni<sub>2</sub>P and its reactivity. Only with very high levels of P did the element block sites on the catalyst. It was also surmised that P<sup>3-</sup> might act as a base in a manner similar to S<sup>2-</sup> in sulfides. As will be seen, P also forms P–OH groups (from unreduced passivation oxygen), which have acidity and play a role in the binding of intermediates.

Fig. 2 shows the water evolution during the temperature-programmed reduction of phosphate to phosphide for the Ni<sub>2</sub>P/MCM-41 sample compared to a Ni<sub>2</sub>P/SiO<sub>2</sub> of lower surface. The onset temperature of reduction for both samples is 750 K (477 °C). However, the MCM-41-supported Ni<sub>2</sub>P catalyst requires a higher reduction temperature indicating a stronger interaction of Ni and phosphorus in smaller crystallites. This was shown previously and confirmed by elemental analysis of fresh Ni<sub>2</sub>P/SiO<sub>2</sub> and Ni<sub>2</sub>P/MCM-41. The MCM-41-supported sample retained more phosphorus even though a higher reduction temperature was utilized as compared to the SiO<sub>2</sub>-supported sample [25].

The reduction of the sample was also followed by Ni K-edge XANES, as shown in Fig. 3. The arrows indicate the shifts in absorbance (μt) during the course of reduction. The major feature is the white line peak at 8345.6 eV, which decreases in intensity with reduction. This is expected, as the white line is indicative of the density of unoccupied electronic states [47,48], which will be decreased by reduction. The peak after the white line at 8372.8 eV is part of the XANES structure, while peaks at 8393.0, and 8426.9 eV, are due to the onset of the EXAFS oscillations. The pre-edge feature at 8330.9 eV is sensitive to Ni symmetry and coordination number changes. This feature will be examined closely later on.

The reduction of the sample was monitored by following the intensity of the absorbance at 8330.9 eV as shown in Fig. 4. The absorbance signal starts increasing significantly after 120 min of reduction, which corresponds to a temperature of 750 K (477 °C).

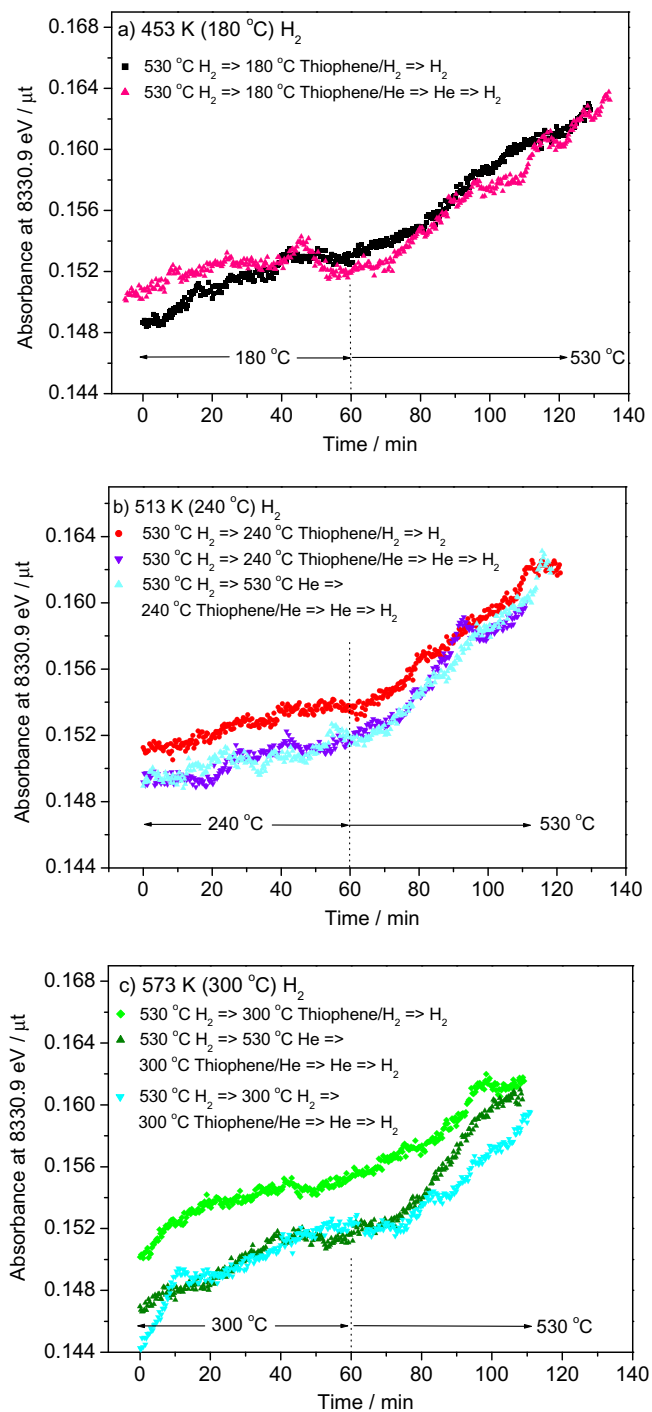


Fig. 15. XANES measurements of the adsorbed thiophene undergoing TPR in H<sub>2</sub>. (a) Reaction at 453 K (180 °C). (b) reaction at 513 K (240 °C), and (c) reaction at 573 K (300 °C).

This is in agreement with the TPR data of Fig. 2, and indicates that the signal at 8330.9 eV can be used to follow the state of the Ni atoms in the sample. An increase in absorbance corresponds to a decrease in oxidation state as well as a decrease in coordination number (due to the removal of oxygen atoms).

The BET specific surface area and CO chemisorption uptake of the MCM-41-supported Ni<sub>2</sub>P sample are listed in Table 1. The BET surface area was much lower than that of the fresh siliceous MCM-41 support. This could be due to filling of micro and/or mesopores upon incorporation of the active phase or because of sintering at the elevated temperatures used in the synthesis. Analysis of the sample was also carried out using extended X-ray absorption fine-structure. Curve fitting analysis of the reduced catalyst using feff parameters gave a Ni–P coordination number of 3.3 ( $R = 0.222$  nm) and a Ni–Ni coordination of 2.8 ( $R = 0.254$  nm). The low Ni–Ni coordination number is consistent with small particle sizes. Previous work showed that the higher the surface area of the support the smaller the particle sizes [18,20].

Fig. 5 shows the powder XRD pattern of the reduced MCM-41-supported Ni<sub>2</sub>P catalyst after passivation. The top panel shows the diffraction pattern of a reference Ni<sub>2</sub>P/SiO<sub>2</sub> sample for comparison. Both patterns exhibit a broad peak at  $2\theta \sim 22^\circ$  due to the amorphous SiO<sub>2</sub> support and the existence of some amorphous domains in MCM-41 upon impregnation of the active phase. At higher angles the XRD pattern for Ni<sub>2</sub>P/SiO<sub>2</sub> confirms the formation of the Ni<sub>2</sub>P phase with peaks at  $2\theta \sim 41^\circ, 45^\circ, 48^\circ,$  and  $55^\circ$ . The phase corresponds to hexagonal Ni<sub>2</sub>P which adopts the Fe<sub>2</sub>P structure with space group P<sub>62m</sub> [49]. The pattern of a reference Ni<sub>2</sub>P from the powder diffraction file (PDF 3-953) is also presented in the bottom panel [50]. For the Ni<sub>2</sub>P/MCM-41 sample no peaks attributable to the Ni<sub>2</sub>P phase are observed due to the high surface area of the support. This verifies the formation of very small Ni<sub>2</sub>P crystallites and high dispersion of the active phase.

Fig. 6 compares the powder XRD patterns of the calcined MCM-41 support and the freshly prepared Ni<sub>2</sub>P/MCM-41 catalyst. The MCM-41 support exhibits an intense line at  $2\theta \sim 2.5^\circ$  and three weak diffraction lines at  $2\theta \sim 4.1^\circ, 4.6^\circ,$  and  $6.1^\circ$  from the (1 0 0), (1 1 0), (2 0 0), and (2 1 0) planes, respectively, characteristic of hexagonal MCM-41 [51]. Impregnation of Ni<sub>2</sub>P on MCM-41 leads to a decrease in intensity and broadening of the (1 0 0) reflection and disappearance of the higher order reflections. This suggests partial destruction of the hexagonal pore arrangement and indicates that the local structure of impregnated MCM-41 is less uniform than pure siliceous MCM-41. However, the retention of some of the MCM-41 peaks indicates that the framework structure does not deteriorate seriously during the synthesis.

#### 4.2. Prior studies of reaction mechanism

Several studies on thiophene HDS have suggested that the major pathway is direct hydrogenolysis of C–S bonds to form 1,3-butadiene, which is subsequently hydrogenated to butenes and butane [52,53] (Scheme 1). A concerted mechanism in which thiophene is directly desulfurized to butenes has also been proposed. The authors concluded that C–S bond cleavage and hydrogenation occurred on the same site and intermediates (diene) reacted faster than they desorbed [54]. However, direct cleavage of C–S bonds is difficult due to the stability of the heterocyclic aromatic ring. As a result, full or partial hydrogenation of the heterocyclic ring has been considered advantageous before C–S bond cleavage [26,55].

Many other studies have advocated hydrogenation of the aromatic heterocyclic ring to form tetrahydrothiophene prior to C–S bond cleavage [26,56,57]. Tetrahydrothiophene can then be desulfurized by transfer of  $\beta$ -hydrogens to the sulfur atom with concomitant cleavage of C–S bonds to yield 1,3-butadiene [58]. Butadiene is subsequently hydrogenated to butenes. Conversely, direct ring

opening and removal of sulfur from tetrahydrothiophene by classic organic mechanisms (S<sub>N</sub>2 and/or E2) may also be possible. Moser and co-workers have shown that butenes could also be formed by the decomposition of tetrahydrothiophene and not only via hydrogenation of 1,3-butadiene. The authors proposed a ring opening mechanism of tetrahydrothiophene by  $\beta$ -hydrogen elimination to form a surface butene thiolate intermediate. Further reaction of the intermediate included rapid C–S bond hydrogenolysis to yield butenes or a slow second  $\beta$ -hydrogen elimination leading to 1,3-butadiene formation [59]. Under atmospheric pressure, however, tetrahydrothiophene is typically not observed as a reaction intermediate [60].

Partially hydrogenated thiophene molecules such as 2,3-dihydrothiophene (2,3-DHT) and 2,5-dihydrothiophene (2,5-DHT) have also been proposed as possible intermediates [55,61,62]. Several studies have observed the formation of these intermediates at low pressures during the HDS of thiophene. Hensen et al. [57] studied the HDS of thiophene over carbon-supported transition metal sulfides at atmospheric pressure and observed the formation of 2,3-DHT. The 2,3-DHT intermediate was found to undergo further reaction by desulfurization, isomerization to 2,5-DHT or rapid hydrogenation to tetrahydrothiophene. The authors concluded that the yield of the partially hydrogenated intermediates depended on the HDS activity of the catalyst – low activity catalysts gave rise to large amounts while catalysts with high HDS activities yielded very small amounts. Several theoretical studies have also shown that formation of dihydrothiophene intermediates is probable prior to C–S bond cleavage [63,64].

#### 4.3. Infrared measurements

The FTIR data in Figs. 7–9 obtained in He flow show great similarity between the pure MCM-41 and the Ni<sub>2</sub>P/MCM-41 and indicate that thiophene is adsorbed extensively on the MCM-41 support except at the lowest temperature for the Ni<sub>2</sub>P/MCM-41. The mode of bonding of the thiophene is molecular in both cases. In Fig. 8 for Ni<sub>2</sub>P/MCM-41 in 1 mol% thiophene/He flow the two absorbance bands at 3742 and 3665 cm<sup>-1</sup> that appear as negative features correspond to surface hydroxyl groups of siliceous MCM-41 on the support and P–OH functionalities, on the support and the active phase [65]. The broad background band between 3600 and 2800 cm<sup>-1</sup> is due to hydrogen-bond interactions. For all spectra, because of the background subtraction a decrease in intensity of a negative band with increasing temperature indicates a recovering of the corresponding species. The opposite applies to positive features in the spectra. In all cases as temperature increases the features due to adsorbed thiophene decrease in intensity and those due to surface OH groups recover due to their desorption. It is surprising to note that the band for P–OH at 3665 cm<sup>-1</sup> recovers faster since these hydroxyl groups are expected to be more acidic than Si–OH. This may indicate that the role of P–OH is not of an acid but of a hydrogenating species similar to S–H.

In Figs. 7 and 8 the features in the 3200–3000 cm<sup>-1</sup> are assigned to aromatic  $\nu_{C-H}$  absorbances while the weak features in the 3000–2800 cm<sup>-1</sup> region are attributed to aliphatic  $\nu_{C-H}$  modes [66] of physisorbed thiophene. In Fig. 9 for Ni<sub>2</sub>P/MCM-41 in 1 mol% thiophene/He flow the main spectral features are located at 1611, 1584, 1574, 1541, 1491, and 1450 cm<sup>-1</sup> and are in the  $\nu_{(C=C)_{sym}}$  region with additional bands at 1420, 1410, and 1400 cm<sup>-1</sup>. Features at 1653, 1636, 1560, and 1506 cm<sup>-1</sup> are clearly observed at 393 K (120 °C). Upon highlighting the  $\nu_{(C=C)_{sym}}$  region a weak band at 1437 cm<sup>-1</sup> was also observed at 393 K (120 °C). The features at 1437, 1420, 1410, and 1400 cm<sup>-1</sup> have been assigned to the symmetric stretching modes of the C=C bonds of thiophene (mode  $\nu_3$ ) [67,68]. It is recognized that the  $\nu_{(C=C)_{sym}}$  absorbances of thiophene are sensitive to the bonding mode of thiophene adsorbed on the

catalyst surface [69,70]. The absorbance bands at 1437 and 1420  $\text{cm}^{-1}$  can be reasonably assigned to thiophene coordinated via its sulfur atom ( $\eta^1(\text{S})$  mode, Scheme 2) to coordinative unsaturated (cus) Ni sites of the active phase and Si–OH sites on the MCM-41 support, respectively. Bussell and co-workers [67,70] studied thiophene adsorption on sulfided Mo/ $\gamma$ - $\text{Al}_2\text{O}_3$ , Rh/ $\gamma$ - $\text{Al}_2\text{O}_3$ , and  $\gamma$ - $\text{Al}_2\text{O}_3$  using FTIR and temperature-programmed desorption. Absorbance features at 1431 and 1420  $\text{cm}^{-1}$  were observed and assigned to  $\eta^1(\text{S})$  bonded thiophene to Mo cus and Al cus, respectively. Similar conclusions were made for thiophene adsorbed on  $\text{Mo}_2\text{N}/\gamma$ - $\text{Al}_2\text{O}_3$  by Li and co-workers [71]. It should be noted that some bands in the region 1600–1450  $\text{cm}^{-1}$  could also be due to incomplete subtraction of the gas-phase thiophene contribution or water in the optical bench, although the latter is degassed. The band at 1620  $\text{cm}^{-1}$  could be due to an adsorbed water impurity from the gas carrier.

For thiophene adsorption on MCM-41 (Fig. 7), the feature at 1420  $\text{cm}^{-1}$  is observed at all temperatures while the feature at 1437  $\text{cm}^{-1}$  is not present. For the  $\text{Ni}_2\text{P}/\text{MCM-41}$  sample, a new low intensity feature at 1437  $\text{cm}^{-1}$  is clearly observed. Upon degassing, the band at 1437  $\text{cm}^{-1}$  is retained up to 513 K (240 °C) while the band at 1420  $\text{cm}^{-1}$  is rapidly diminished. (spectra not shown for brevity) The low intensity of the band at 1437  $\text{cm}^{-1}$  due to  $\eta^1(\text{S})$ -bonded thiophene on Ni cus sites is likely due to the relatively high adsorption temperature and, as discussed briefly below, some decomposition of thiophene on the catalyst surface. The bands at 1400 and 1410  $\text{cm}^{-1}$  are assigned to thiophene hydrogen bonded through its sulfur atom to different surface hydroxyl groups on the support ( $\text{C}_4\text{H}_4\text{S}\cdots\text{HO-Si}$ ) [72]. An increase in temperature led to a rapid decrease in the intensity of bands located at 1653, 1636, 1560, 1506, and 1437  $\text{cm}^{-1}$ . The intensities of the spectral features centered at 1611, 1491, and 1450  $\text{cm}^{-1}$  were observed to increase slightly upon heating to 593 K (320 °C) and decrease at higher temperatures. All other bands were maintained up to 723 K (450 °C).

A dramatic change was observed when the carrier gas was switched from He to  $\text{H}_2$ . Fig. 10 shows the FTIR spectra at high wavenumbers of thiophene adsorbed on  $\text{Ni}_2\text{P}/\text{MCM-41}$  in 1 mol% thiophene/ $\text{H}_2$  flow with the right panel highlighting the  $\nu_{\text{C-H}}$  region of the spectra. Three new bands with high intensity appeared at 2953, 2918, and 2876  $\text{cm}^{-1}$ , and grew in intensity with rise in temperature from 393 to 553 K (120 to 280 °C), and then decreased. This region corresponds to aliphatic  $\nu_{\text{CH}}$  modes, so clearly some hydrogenation of thiophene occurred. The increase and then decrease in intensity of these bands is unusual, and indicates that they are due to hydrogenated reactive intermediates that are formed in  $\text{H}_2$ , and then desorb at higher temperatures.

Two negative bands at 3740 and 3667  $\text{cm}^{-1}$  due to consumption of hydroxyl groups were again observed, indicating that interaction with these groups was occurring. As with He the feature at 3740  $\text{cm}^{-1}$  was retained up to 723 K (450 °C) while the intensity of the feature at 3667  $\text{cm}^{-1}$  decreased with increasing temperature. The weak features due to aromatic  $\nu_{\text{CH}}$  modes at 3136, 3125, 3107, 3098, 3090, and 3080  $\text{cm}^{-1}$  were again observed. These features were observed in the 3000–2800  $\text{cm}^{-1}$  range under He flow (Fig. 8), although much weaker in intensity. In He flow, the appearance of aliphatic  $\nu_{\text{CH}}$  modes is likely attributable to some decomposition of thiophene on the catalyst surface and formation of adsorbed  $\text{C}_4$  hydrocarbons. Such decomposition under inert conditions has been observed upon adsorption of thiophene on Ni single crystals, even at low temperatures (150 K) [73,74]. Above 553 K (280 °C) the intensity of these bands were observed to decrease with increasing temperature up to 723 K (450 °C). This is due to desorption, as expected.

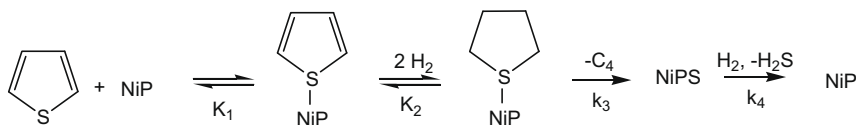
Fig. 11 shows the corresponding FTIR spectra of thiophene adsorbed on  $\text{Ni}_2\text{P}/\text{MCM-41}$  in 1 mol% thiophene/ $\text{H}_2$  flow in the low

wavenumber region. The right panel expands the  $\nu_{(\text{C=C})_{\text{sym}}}$  region of the spectra. The most significant result was the finding of a band at 1464  $\text{cm}^{-1}$ , which appears as a shoulder on the feature at 1449  $\text{cm}^{-1}$ . This band first grew in intensity with heating from 393 to 553 K (120 to 280 °C), but then diminished rapidly at higher temperatures. Again, this is not the expected behavior for a species that is simply adsorbed. It indicates that the species is a hydrogenated reactive intermediate that is formed under hydrogen, and then desorbs at higher temperature. It is probably associated with the same aliphatic  $\nu_{\text{CH}}$  modes at 2953, 2918, and 2876  $\text{cm}^{-1}$  in Fig. 10, which displayed the same temperature response. The band at 1464  $\text{cm}^{-1}$  can be reasonably assigned to the asymmetric  $\text{CH}_2$  scissoring (mode  $\nu_{21}$ ) of tetrahydrothiophene (THT) [75] with corresponding  $\nu_{\text{CH}}$  bands. It should be noted that another possibility is that the growth and decline in intensity could also be due to a readorption phenomenon, but this is unlikely as it is not observed for other species in the spectra taken under He.

There were other hydrogenated species formed. Fig. 11 also shows features at 1491 and 1449  $\text{cm}^{-1}$ , which are much more intense in  $\text{H}_2$  than in He. These, however, simply diminish in intensity as temperature is raised, and correspond to standard adsorbed species. The rest of the main spectral features located at 1638, 1601, 1491, 1449, 1420, 1410, and 1400  $\text{cm}^{-1}$  are very similar to those obtained under He flow. Again, an increase in the temperature led to a decrease in the intensity of bands located at 1653, 1638, 1626, 1601, 1506, 1491, 1449, and 1437  $\text{cm}^{-1}$  while all other bands were retained up to 723 K. This was the same as in He, and the bands are due to decomposition products of thiophene on the MCM-41 support.

The behavior of the adsorbed species was studied by abruptly removing thiophene from the feed and switching to pure  $\text{H}_2$ . As shown in Scheme 1 the products of thiophene HDS are typically 1,3-butadiene, 1-butene, 2-butene (cis- and trans-), and butane. In order to interpret the resulting spectra during thiophene reaction, Li and co-workers [71] employed in situ FTIR and adsorption of these HDS products over  $\text{Mo}_2\text{N}/\gamma$ - $\text{Al}_2\text{O}_3$ . For the desulfurized products of thiophene reaction over the  $\text{Ni}_2\text{P}/\text{MCM-41}$  sample, a similar interpretation can be applied. Over a reduced  $\text{Mo}_2\text{N}/\gamma$ - $\text{Al}_2\text{O}_3$  catalyst, the three butene products exhibited nearly identical absorbance bands at 3010, 2965, 2922, 2860, 1619, 1612, 1452, 1408, and 1381  $\text{cm}^{-1}$ . The observed surface species were attributed to  $\pi$ - and  $\sigma$ -bonded butenes [76,77]. Adsorption of 1,3-butadiene gave absorbance bands located at 3010, 3005, 2920, 2850, 1616, 1565, 1490, 1457, 1417, and 1378  $\text{cm}^{-1}$ . These features were assigned to  $\pi$ -adsorbed butadiene and  $\sigma$ -bonded and dehydrogenated butadiene species on the catalyst surface [76]. Another possibility is that an irreversible formation of adsorbed butadiene as a carboxylate with bands reported at 2958, 2875, 1560, and 1450  $\text{cm}^{-1}$  [78] occurs on the phosphate component. For reaction of thiophene over  $\text{Ni}_2\text{P}/\text{MCM-41}$ , the strong IR bands in the aliphatic  $\nu_{\text{C-H}}$  region (3000–2800  $\text{cm}^{-1}$ ) and the intense bands centered at 1549, 1491, and 1449  $\text{cm}^{-1}$  can be assigned to vibrations of  $\text{CH}_2$  and  $\text{CH}_3$  groups of adsorbed  $\text{C}_4$  hydrocarbons [79]. Analogous to the thiophene reaction on the nitride catalyst, the intense band at 1491  $\text{cm}^{-1}$  can be assigned to a significant amount of surface-adsorbed 1,3-butadiene. The band at 1491  $\text{cm}^{-1}$  is likely due to di- $\pi$ -adsorbed 1,3-butadiene ( $\nu_{\text{C=C}}$  mode) while the band at 1549  $\text{cm}^{-1}$  can be tentatively assigned to a singularly  $\pi$ -bonded 1,3-butadiene species ( $\nu_{\text{C=C}}$  mode) [76]. The feature at 1449  $\text{cm}^{-1}$  is likely due to both  $\pi$ - and  $\sigma$ -bonded butenes. However, for 1-butene, Li and co-workers [76] gave evidence that this band is likely attributable to the presence of a  $\sigma$ -allyl butene species ( $\delta(\text{CH}_3)_{\text{as}}/\delta(\text{CH}_2)_{\text{as}}$ ) via isomerization.

Overall, the FTIR results are consistent with a reaction sequence for thiophene HDS as shown in Scheme 3. Thiophene is adsorbed and forms a  $\eta^1(\text{S})$ -bonded complex with nickel. This is



**Scheme 3.** Simplified surface HDS mechanism showing adsorbed tetrahydrothiophene and the surface phosphosulfide.

hydrogenated to form the tetrahydrothiophene species with aliphatic  $\nu_{\text{CH}}$  bands at 2953, 2918, and 2876  $\text{cm}^{-1}$  which increased in intensity from 393 to 553 K (120 to 280 °C) and decreased at higher temperatures. Analogously, the feature at 1464  $\text{cm}^{-1}$  (Figs. 11 and 12) exhibits a similar temperature dependence and can be reasonably assigned to the same species. The tetrahydrothiophene increased in concentration as temperature was increased from 393 to 553 K because it is formed as a result of two sequential processes of different temperature dependence. At high temperature, the cleavage of C–S bonds to form the surface phosphosulfide species accelerates relative to the hydrogenation step, and the concentration of the tetrahydrothiophene surface species diminishes. Other species observed like molecularly adsorbed thiophene and the hydrocarbons probably reside on the support.

The above-mentioned scheme assumes that the tetrahydrothiophene decomposition (step 3) and the phosphosulfide hydrogenation (step 4) are kinetically significant, and that thiophene adsorption and hydrogenation are equilibrated. This gives rise to the following rate expression:

$$\gamma = \frac{k_2 K_1 (\text{H}_2)^2 (\text{thiophene})}{1 + (k_2/k_3) K_1 (\text{H}_2)^2 (\text{thiophene})} \quad (3)$$

$$\text{Rate} = k' (\text{Thiophene})^\alpha (\text{H}_2)^{2\alpha} \gamma = k' (\text{H}_2)^{2\alpha} (\text{thiophene})^\alpha$$

$$k' = (L) k_3 [K_1 K_2]^\alpha \quad (4)$$

Rate expressions in which the reaction order in  $\text{H}_2$  was twice the order in thiophene have been proposed previously, especially for catalysts with high hydrogenation activity. Hensen et al. [80] measured the kinetics of thiophene HDS at 623 K (350 °C) in the presence of 1 kPa  $\text{H}_2\text{S}$  over several C-supported transition metal sulfides. The authors determined that the reaction order in  $\text{H}_2$  was approximately twice the order in thiophene for sulfided Ru/C, Rh/C, and Pd/C.

#### 4.4. XANES measurements

The infrared spectroscopy studies discussed in the previous section gave evidence for the existence of a reactive intermediate, tetrahydrothiophene, on the surface of the catalyst, but gave no indication of where it was bonded and of its reactivity. This is addressed in this section where studies with X-ray absorption near-edge spectroscopy (XANES) at the Ni K-edge are used to follow the interaction of the intermediate with Ni centers. The absorbance at the pre-edge feature at 8330.9 eV is sensitive to changes in Ni symmetry and coordination number, and was used to follow the adsorption and reaction processes. It is well known that the intensity of the pre-edge peaks for K-edge transitions decreases as coordination increases, for example, in going from tetrahedral to octahedral Ti coordination [81]. Thus, adsorption tends to decrease the intensity of the feature, and desorption to increase it. XANES data are much less sensitive to temperature than EXAFS measurements because they are not dependent on vibrational movement, so XANES is an appropriate tool to probe adsorption at high temperature.

When a freshly reduced  $\text{Ni}_2\text{P}/\text{MCM-41}$  sample is exposed to thiophene/ $\text{H}_2$  mixtures the absorbance at 8330.9 eV shows a rapid

decrease to steady values as indicated in Fig. 13. (The spike at time zero is an artifact due to the switch in gas streams.) Referring to Scheme 3, this is due to the interaction of the sulfur atoms of thiophene with the Ni centers, whose coordination increases. However, it should be noted that the sulfur atoms could be due to thiophene, tetrahydrothiophene, or the surface phosphosulfide. The greater drop in absorbance with temperature indicates that the coverage in sulfur species at the surface is higher at higher temperatures. This is in the same temperature range (453–573 K, 180–300 °C) as the FTIR measurements discussed earlier which showed the growth of bands assigned to tetrahydrothiophene (THT). Thus, the increase in coverage with temperature detected by XANES, which is unusual since most adsorbed species would decline in concentration, is consistent with the adsorbed THT or the formation of a surface phosphosulfide.

Transient experiments at short times of thiophene in  $\text{H}_2$  and He carriers are shown in Fig. 14. The decline in absorbance at 8330.9 eV is again indicative of adsorption of a sulfur species. As just discussed, the larger decline at higher temperatures is consistent with the surface sulfur. It is possible to roughly estimate the percentage decline in the initial stages of the absorbance by taking slopes ( $d\mu/dt$ ) as indicated in the figures. Since the absorbance is related to the thiophene coverage, the slopes are indicative of the rates of thiophene adsorption ( $d\theta/dt$ ).

For the thiophene in He curve, the change in coverage with time gives the net rate of adsorption

$$\left(\frac{d\theta}{dt}\right)_{\text{He}} = r_{\text{ads}} - r_{\text{des}} \quad (5)$$

For the thiophene in  $\text{H}_2$  curve, the change in coverage also includes the rate of reaction for the formation of THT or the phosphosulfide (Scheme 3)

$$\left(\frac{d\theta}{dt}\right)_{\text{H}_2} = r_{\text{ads}} - r_{\text{des}} + r_{\text{rxn}} \quad (6)$$

The difference in both quantities can be used to give the rate of reaction for the formation of THT or the phosphosulfide

$$\left(\frac{d\theta}{dt}\right)_{\text{H}_2} - \left(\frac{d\theta}{dt}\right)_{\text{He}} = r_{\text{rxn}} \quad (7)$$

A limitation in this analysis is that the absorbance,  $\mu t$ , has not been related quantitatively to the coverage,  $\theta$ . However, assuming linearity, and estimating an approximate correspondence between the percentage values, allows a very rough order-of-magnitude determination. Thus, at 513 K (240 °C) the reaction rate can be calculated to be

$$\left(\frac{d\theta}{dt}\right)_{\text{H}_2} - \left(\frac{d\theta}{dt}\right)_{\text{He}} = 2.2 - 1.6\% \text{ s}^{-1} = 0.6\% \text{ s}^{-1} = 0.006 \text{ s}^{-1} \quad (8)$$

At 573 K (300 °C) the reaction rate can be calculated to be

$$\left(\frac{d\theta}{dt}\right)_{\text{H}_2} - \left(\frac{d\theta}{dt}\right)_{\text{He}} = 4.6 - 3.7\% \text{ s}^{-1} = 0.9\% \text{ s}^{-1} = 0.009 \text{ s}^{-1} \quad (9)$$

Steady-state reactivity data were also measured, as will be described in the next section. The calculated values above are close to the measured turnover frequencies of  $0.0071 \text{ s}^{-1}$  at 513 K (240 °C) and  $0.0082 \text{ s}^{-1}$  at 573 K (300 °C). The close correspondence

in these values indicates that the formation of the Ni–S intermediate (due to either adsorbed THT or a surface phosphosulfide) is a key step in the reaction.

In previous work [18,22,46] it was suggested that the active phase of Ni<sub>2</sub>P consisted of a phosphosulfide. It was therefore of interest to check the nature of the sulfur species on the surface of Ni<sub>2</sub>P/MCM-41.

Fig. 15 shows XANES traces obtained in isothermal and temperature-programmed experiments where adsorbed thiophene is desorbed. In this case the absorbance increases, which indicates a decline in Ni–S coordination. The left part of Fig. 15a) shows the signals when flows of thiophene in H<sub>2</sub> at 453 K (180 °C) are changed to pure H<sub>2</sub>. In the isothermal region at 453 K (180 °C) the absorbance increases and reaches a plateau, indicating that adsorbed thiophene (the tetrahydrothiophene intermediate) has desorbed. When the temperature is ramped to 803 K (530 °C) the absorbance increases again. This is indicative of the removal of further sulfur, and this is interpreted as removal of the phosphosulfide sulfur. Similar results are presented in Fig. 15b) where the left part of the figure shows the signals when flows of thiophene in H<sub>2</sub> and He at 513 K (240 °C) are changed to pure H<sub>2</sub>. In the isothermal portion at 513 K (240 °C) the signals reach a plateau as the adsorbed thiophene (tetrahydrothiophene) is desorbed. When the temperature is then ramped to 803 K (530 °C) the absorbance increases in the same manner for all samples. Again, the interpretation is that this corresponds to the removal of the phosphosulfide sulfur. The experiments are repeated in Fig. 15c) where the left part of the figure shows the signals in flows of thiophene in H<sub>2</sub> and He at 573 K (300 °C) which are changed to pure H<sub>2</sub>. In the isothermal region at 573 K (300 °C) the signals reach a plateau as the adsorbed thiophene (tetrahydrothiophene) is desorbed. When the temperature is ramped to 803 K (530 °C) the absorbance increases as the phosphosulfide sulfur is removed.

The conclusion of this work is that there are two types of sulfur that are observable by XANES. One type is associated with an adsorbed sulfur-containing species, which is suggested to be tetrahydrothiophene, from the observation of aliphatic C–H stretches and CH<sub>2</sub> scissoring stretches in the FTIR spectrum. The other type is a phosphosulfide sulfur that is strongly held on the surface of the Ni<sub>2</sub>P catalyst. Dynamic experiments show that the adsorbed sulfur species is a reactive intermediate because it reacts at the same rate as the steady-state rate.

#### 4.5. Steady-state HDS activity

Table 2 summarizes the thiophene HDS results for the Ni<sub>2</sub>P/MCM-41 sample as a function of temperature at atmospheric pressure. The activity tests were conducted with the same amount of catalyst charged to the reactor (0.047 g) as for the transient XANES measurements. Additionally, all experiments were conducted at the same weight hourly space velocity (WHSV = 22.2 h<sup>-1</sup>). The conversion of thiophene was observed to increase with increasing temperature, as expected. The selectivity for HDS products was 100% at all reaction temperatures and consisted of entirely C<sub>4</sub> hydrocarbons (butenes and butane). Table 2 also presents the turnover frequencies for the Ni<sub>2</sub>P/MCM-41 catalyst in the HDS of thiophene as a function of temperature at atmospheric pressure. Using

the measured thiophene conversions, the TOFs for thiophene reaction were calculated with Equation 2 based on the CO uptake value for the MCM-41-supported Ni<sub>2</sub>P catalyst (Table 1). The measured TOFs for thiophene HDS at 513 and 573 K (240 and 300 °C) are in good agreement with the values obtained in the transient XANES measurements. It is recognized that the TOFs are obtained at high conversion and therefore are average values over the integral reactor. However, since the kinetics of the reaction for similar systems [79] do not indicate product inhibition, the TOFs probably represent the surface processes depicted in Scheme 3.

The apparent activation energy for the HDS of thiophene was obtained from the slope of an Arrhenius plot, and the calculated apparent activation energy was 6.2 kJ mol<sup>-1</sup>. This is a low value, but can be explained from the kinetic expression derived for Scheme 3. The apparent activation energy is given by  $E_{app} = E_3 + \Delta H_1 + \Delta H_2$ , and because the equilibria represent exothermic adsorption and hydrogenation steps their effect is to reduce the apparent activation energy. Such an effect has been reported earlier for thiophene HDS [60].

Absence of internal diffusion limitations was checked using the Weisz–Prater criterion [82]. It was confirmed that at the highest temperature used (573 K, 300 °C) the quantity  $R^2r/C_sD_e$  had a value of 0.31, where  $R$  is the thickness of the catalyst wafer (0.030 cm),  $r$  is the volumetric rate ( $1.8 \times 10^{-6}$  mol cm<sup>-3</sup> s<sup>-1</sup>),  $C_s$  is the thiophene concentration ( $5.3 \times 10^{-8}$  mol cm<sup>-3</sup>), and  $D_e$  is the diffusivity of thiophene (0.10 cm<sup>2</sup> s<sup>-1</sup>). The value satisfied the criterion,  $R^2r/C_sD_e < 1$ , suggesting no internal diffusion limitations or concentration gradient within the catalyst wafer.

## 5. Conclusions

The hydrodesulfurization (HDS) of thiophene was studied on Ni<sub>2</sub>P/MCM-41 using in situ Fourier transform infrared (FTIR) spectroscopy and near-edge X-ray absorption fine-structure (XANES). The FTIR measurements showed the appearance of an adsorbed hydrogenated species, assigned to tetrahydrothiophene, when thiophene and hydrogen were passed over the catalyst. The intensity of the FTIR bands rose with temperature and then declined, indicating that the steps for the formation and reaction of the species had different temperature dependencies. In situ XANES measurements confirmed the presence of a surface sulfur species, which could be tetrahydrothiophene or a phosphosulfide phase, through the monitoring of a signal that responded to the formation of Ni–S bonds. Dynamic experiments with XANES in which the sulfur species was desorbed in He and H<sub>2</sub> allowed the estimation of its rate of reaction at two temperatures. These rates corresponded closely to the overall turnover frequency of the reaction. Additional XANES experiments showed that the surface of the Ni<sub>2</sub>P/MCM-41 was likely a phosphosulfide, in agreement with the past determinations.

## Acknowledgments

This work was supported by the US Department of Energy, Office of Basic Energy Sciences, through Grant DE-FG02-963414669 and JST Grant-in-Aid for Scientific Research (Category S, No. 16106010). The XAFS experiments were conducted under approval of PF-PAC (Project No. 2008G129).

## References

- [1] S.T. Oyama, T. Gott, H. Zhao, Catal. Today 143 (2009) 94.
- [2] S.E. Eijsbouts, J.A.R. van Veen, E.J.M. Hensen, G. Mul. (Eds.), Fourth International Symposium on Molecular Aspects of Catalysis by Sulfides, Doorn, The Netherlands, May 13–17, 2007 (Catal. Today 130 (2008)).
- [3] K.P. Zhdanova, M.A. Lur'e, I.Z. Kurets, E.Kh. Kim, F.K. Shmidt, Kinet. Catal. 41 (2000) 892.

**Table 2**

Steady-state thiophene HDS results.

Sample	Temperature (K)	Conversion (%)	TOF (s <sup>-1</sup> )
Ni <sub>2</sub> P/MCM-41	573	80	0.0082
	513	69	0.0071
	453	57	0.0058

- [4] Y.-K. Lee, S.T. Oyama, *J. Catal.* 239 (2006) 376.
- [5] Y. Kanda, T. Aizawa, T. Kobayashi, Y. Uemichi, S. Namba, M. Sugioka, *Appl. Catal., B* 77 (2007) 117.
- [6] W. Wu, Z. Wu, Z. Feng, P. Ying, C. Li, *Phys. Chem. Chem. Phys.* 6 (2004) 5596.
- [7] M.A. Larrubia, A. Gutiérrez-Alejandre, J. Ramirez, G. Busca, *Appl. Catal., A* 224 (2002) 167.
- [8] Z. Wu, Y. Chu, S. Yang, Z. Wei, C. Li, Q. Xin, *J. Catal.* 194 (2000) 23.
- [9] V. Schwartz, M. Sun, R. Prins, *J. Phys. Chem. B* 106 (2002) 2597.
- [10] M. Taniguchi, D. Imamura, H. Ishige, Y. Ishii, T. Murata, M. Hidai, T. Tatsumi, *J. Catal.* 187 (1999) 139.
- [11] N. Frizi, P. Blanchard, E. Payen, P. Baranek, M. Rebeilleau, C. Dupuy, J.P. Dath, *Catal. Today* 130 (2008) 272.
- [12] Y. Yoshimura, M. Toba, T. Matsui, M. Harada, Y. Ichihashi, K.K. Bando, H. Yasuda, H. Ishihara, Y. Morita, T. Kameoka, *Appl. Catal., A* 322 (2007) 152.
- [13] K.K. Bando, T. Kawai, K. Asakura, T. Matsui, L.L. Bihan, H. Yasuda, Y. Yoshimura, S.T. Oyama, *Catal. Today* 111 (2006) 199.
- [14] R. Cattaneo, T. Weber, T. Shido, R. Prins, *J. Catal.* 191 (2000) 225.
- [15] C. Stinner, R. Prins, T. Weber, *J. Catal.* 191 (2000) 438.
- [16] D.C. Phillips, S.J. Sawhill, R. Self, M.E. Bussell, *J. Catal.* 207 (2002) 266.
- [17] S.T. Oyama, *J. Catal.* 216 (2003) 343.
- [18] S.T. Oyama, X. Wang, Y.-K. Lee, W.-J. Chun, *J. Catal.* 221 (2004) 263.
- [19] S.T. Oyama, X. Wang, F. Requejo, T. Sato, Y. Yoshimura, *J. Catal.* 209 (2002) 1.
- [20] Y. Shu, Y.-K. Lee, S.T. Oyama, *J. Catal.* 236 (2005) 112.
- [21] Y.-K. Lee, Y. Shu, S.T. Oyama, *Appl. Catal.* 322 (2007) 191.
- [22] T. Kawai, S. Sato, W.J. Chun, K. Asakura, K.K. Bando, T. Matsui, Y. Yoshimura, T. Kubota, Y. Okamoto, Y.K. Lee, S.T. Oyama, *Chem. Lett.* 32 (2003) 956.
- [23] T. Kawai, S. Sato, W.J. Chun, K. Asakura, K.K. Bando, T. Matsui, Y. Yoshimura, T. Kubota, Y. Okamoto, Y.K. Lee, S.T. Oyama, *Phys. Scripta* (2004) T115.
- [24] T. Kawai, K.K. Bando, Y.-K. Lee, S.T. Oyama, W.J. Chun, K. Asakura, *J. Catal.* 241 (2006) 20.
- [25] S.T. Oyama, Y.-K. Lee, *J. Catal.* 258 (2008) 393.
- [26] H. Topsøe, B.S. Clausen, F.E. Massoth, *Hydrotreating Catalysis-Science and Technology*, Springer-Verlag, Berlin, 1996.
- [27] M.J. Girgis, B.C. Gates, *Ind. Eng. Chem. Res.* 30 (1991) 2021.
- [28] R. Shafi, G.J. Hutchings, *Catal. Today* 59 (2000) 423.
- [29] M. Neurock, R.A. van Santen, *J. Am. Chem. Soc.* 116 (1994) 4427.
- [30] R.J. Angelici, *Polyhedron* 16 (1997) 3073.
- [31] R.J. Angelici, *Bull. Soc. Chim. Belg.* 104 (1995) 265.
- [32] P.C.H. Mitchell, D.A. Green, E. Payen, J. Tomkinson, S.F. Parker, *Phys. Chem. Chem. Phys.* 1 (1999) 3357.
- [33] C. Bianchini, J.A. Casares, R. Osman, D.I. Pattison, M. Peruzzini, R.N. Perutz, F. Zanobini, *Organometallics* 16 (1997) 4611.
- [34] L. Dong, S.B. Duckett, K.F. Ohman, W.D. Jones, *J. Am. Chem. Soc.* 114 (1992) 151.
- [35] S. Luo, T.B. Rauchfuss, Z. Gan, *J. Am. Chem. Soc.* 115 (1993) 4943.
- [36] R. Prins, V.H.J. de Beer, G.A. Somorjai, *Catal. Rev.-Sci. Eng.* 31 (1989) 1.
- [37] B.C. Wiegand, C.M. Friend, *Chem. Rev.* 92 (1992) 491.
- [38] D.R. Huntley, D.R. Mullins, M.P. Wingeier, *J. Phys. Chem.* 100 (1996) 19620.
- [39] S.T. Oyama, W. Li, *Top. Catal.* 8 (1999) 75.
- [40] J.J. Bravo-Suárez, K.K. Bando, J.Q. Lu, M. Haruta, T. Fujitani, S.T. Oyama, *J. Phys. Chem. C* 112 (2008) 1115.
- [41] T. Gott, S.T. Oyama, *J. Catal.* 263 (2009) 359.
- [42] M. Fernández-García, *Catal. Rev.-Sci. Eng.* 44 (2002) 59.
- [43] C.-F. Cheng, D.H. Park, J. Klinowski, *J. Chem. Soc., Faraday Trans.* 93 (1) (1997) 193.
- [44] C.L. Yaws, K.P. Narasimhan, C. Gabbula, *Yaws' Handbook of Antoine Coefficients for Vapor Pressure*, Knovel, 2005.
- [45] K.K. Bando, T. Saito, K. Sato, T. Tanaka, F. Dumeignil, M. Imamura, N. Matsubayashi, H. Shimada, *Top. Catal.* 18 (2002) 59.
- [46] S.T. Oyama, X. Wang, Y.-K. Lee, K. Bando, F. Requejo, *J. Catal.* 210 (2002) 207.
- [47] F.W. Lytle, *J. Catal.* 43 (1976) 376.
- [48] F.W. Lytle, P.S.P. Wei, R.B. Gregor, G.H. Via, J.H. Sinfelt, *J. Chem. Phys.* 70 (1979) 4849.
- [49] S. Rundqvist, *Acta Chem. Scand.* 16 (1962) 992.
- [50] Powder Diffraction Data Files, JCPDS International Center for Diffraction Data, Swathmore, PA, 1992.
- [51] C.T. Kresge, M.E. Leonowicz, W.J. Roth, J.C. Vartuli, J.S. Beck, *Nature* 359 (1992) 710.
- [52] A.E. Hargreaves, J.R.H. Ross, *J. Catal.* 56 (1979) 363.
- [53] K.F. McCarthy, G.L. Schrader, *J. Catal.* 103 (1987) 261.
- [54] A.N. Startsev, V.A. Burmistrov, Y. Yermakov, *Appl. Catal.* 45 (1988) 191.
- [55] E.J. Markel, G.L. Schrader, N.N. Sauer, R.J. Angelici, *J. Catal.* 116 (1989) 11.
- [56] J. Kraus, M. Zdrzil, *React. Kinet. Catal. Lett.* 6 (1977) 475.
- [57] E.J.M. Hensen, M.J. Vissenberg, V.H.J. de Beer, J.A.R. van Veen, R.A. van Santen, *J. Catal.* 163 (1996) 429.
- [58] S. Kolboe, *Can. J. Chem.* 47 (1969) 352.
- [59] W.R. Moser, G.A. Rossetti Jr., J.T. Gleaves, J.R. Ebner, *J. Catal.* 127 (1991) 190.
- [60] A. Borgna, E.J.M. Hensen, L. Coulier, M.H.J.M. de Croon, J.C. Schouten, J.A.R. van Veen, J.W. Niemantsverdriet, *Catal. Lett.* 90 (2003) 117.
- [61] B.T. Carvill, M.J. Thompson, *Appl. Catal.* 75 (1991) 249.
- [62] R.J.C. Osbaldiston, E.J. Markel, *J. Mol. Catal.* 91 (1994) 91.
- [63] C. Rong, X. Qin, *J. Mol. Catal.* 64 (1991) 321.
- [64] P.G. Moses, B. Hinnemann, H. Topsøe, J.K. Nørskov, *J. Catal.* 248 (2007) 188.
- [65] S.T. Oyama, Y.-K. Lee, *J. Phys. Chem. B* 109 (2005) 2109.
- [66] K.A. Layman, M.E. Bussell, *J. Phys. Chem. B* 108 (2004) 15791.
- [67] T.L. Tarbuck, K.R. McCrea, J.W. Logan, J.L. Heiser, M.E. Bussell, *J. Phys. Chem. B* 102 (1998) 7845.
- [68] A.A. El-Azhary, R.H. Hilal, *Spectrochim. Acta* 53 (1997) 1365.
- [69] P. Mills, S. Korlann, M.E. Bussell, M.A. Reynolds, M.V. Ovchinnikov, R.J. Angelici, C. Stinner, T. Weber, R. Prins, *J. Phys. Chem. A* 105 (2001) 4418.
- [70] P. Mills, D.C. Phillips, B.P. Woodruff, R. Main, M.E. Bussell, *J. Phys. Chem. B* 104 (2000) 3237.
- [71] Z. Wu, C. Li, Z. Wei, P. Ying, Q. Xin, *J. Phys. Chem. B* 106 (2002) 979.
- [72] W.W.C. Quigley, H.D. Yamamoto, P.A. Aegerter, G.J. Simpson, M.E. Bussell, *Langmuir* 12 (1996) 1500.
- [73] J.A. Rodriguez, J. Dvorak, A.T. Capitano, A.M. Gabelnick, J.L. Gland, *Surf. Sci.* 429 (1999) L462.
- [74] N.A. Khan, H.H. Hwu, J.G. Chen, *J. Catal.* 205 (2002) 259.
- [75] T.M. El-Gogary, *Spectrochim. Acta, Part A* 57 (2001) 1405.
- [76] Z. Wu, Z. Hao, P. Ying, Z. Wei, C. Li, Q. Xin, *J. Phys. Chem. B* 104 (2000) 12275.
- [77] Z. Wu, C. Li, P. Ying, Z. Wei, Q. Xin, *J. Phys. Chem. B* 105 (2001) 9183.
- [78] F. Can, A. Travert, V. Ruau, J.-P. Gilson, F. Maugé, R. Hu, R.F. Wormsbecher, *J. Catal.* 249 (2007) 79.
- [79] M. Trombetta, G. Busca, S. Rossini, V. Piccoli, U. Cornaro, *J. Catal.* 168 (1997) 334.
- [80] E.J.M. Hensen, H.J.A. Brans, G.M.H.J. Lardinois, V.H.J. de Beer, J.A.R. van Veen, R.A. van Santen, *J. Catal.* 192 (2000) 98.
- [81] F. Farges, G.E. Brown, J.J. Rehr, *Geochim. Cosmochim. Acta* 60 (1996) 3023.
- [82] P.B. Weisz, C.D. Prater, *Adv. Catal. Relat. Subj.* 6 (1954) 143.